Design Project

Master in Mechanical Engineering

Design and analysis of the Engine Reservoir of the Buried Ocean Battery

Author:
Núria Masclans Serrat S4162935

Supervisors:
1st supervisor: Marijn van Rooij
2nd supervisor: Antonis Vakis

December 6, 2020

Preface

This Design Project report is the result of a three months work conducted by the author in collaboration with Ocean Grazer Company and University of Groningen. The project aims to develop and to perform a mechanical analysis of a preliminary design for the Engine Reservoir of the Ocean Battery, a project in progress of Ocean Grazer Company.

I would like to thank my supervisors Marijn van Rooij and Proj. dr. Antonis Vakis for giving me the opportunity to make a contribution in such a promising and sustainable project, and to guide me along all the process. I would also like to express my gratitude to Prof. dr. Wout Prince, whose bright ideas where always of a big help.

Finally, I would like to give very special thanks to my family, who I miss very much.

Núria Masclans Serrat
December 5, 2020

Abstract

Nowadays, the sector of energy production is suffering a significant increase on renewable energy. Therefore, renewable methods for energy storage must be developed accordingly. Ocean Grazer company believes on a renewable, clean and reliable way of storing energy produced by renewable power sources. The company is currently developing the so-call Ocean Battery, a system of flexible and rigid reservoirs based on the principle of storing the produced energy by renewable power plants as potential energy. It is expected to be located on a sea or lake bottom, with a Rigid Reservoir buried on the soil and a Flexible Reservoir laying on the soil surface. Although some research has been developed on the design of the Rigid and Flexible Reservoirs, Ocean Grazer has detected a lack of knowledge regarding the third component of the battery: the Engine Reservoir. The Engine Reservoir is the interconnecting element between the Rigid and Flexible Reservoirs, and it contains the hydro-power components required for energy storage and production. Therefore, the project focuses on providing a first design of the Engine Reservoir. In order to do so, the requirement of the component are identified and the main hydro-power components characterised. Additionally, a study on the medium interaction with the structure is performed, and the relevant loads and momentum are identified and quantified through Matlab and COMSOL models. Finally, the mechanical study is performed, and the design evaluated.

Contents

List of Figures

List of Tables

1 Introduction

The word is suffering a rising need of sustainable, clean and affordable energy. Specially in the field of energy storage, there is a clear predominance of mineral based batteries (such as lithium-based batteries), which contain materials that need to be mined and furthermore they are very difficult to recycle. Ocean Grazer identified this deficiency, and is currently developing a Ocean Battery capable of storing energy in a completely renewable way [7].

The project of the Ocean Battery stated on 2014 within a research group on the University of Groningen. Ocean Grazer company was founded few years after, and nowadays is currently testing in the field the first prototype of the Ocean Battery at small scale. Based on storing energy through potential energy, the Ocean Battery is compatible with all types of power plants, including hybrid power plants. IT must be of high versability to adapt to every implementation requirements, and robust to withstand de extreme pressure conditions of the sea or lake bottom.

2 Problem Definition

As introduced in the Preface, Ocean Grazer company has no preliminary design for the Engine Reservoir of the Ocean Battery. Furthermore, there is a gap on knowledge on the system requirements and on the design parameters of the hydro-power components within the Engine Reservoir. Furthermore, there is no clear description of the mechanical interactions of the Engine Reservoir with the environment and with the other components of the Ocean Battery.

2.1 Problem Statement

From the problem definition introduction, it is clear that Ocean Grazer company requires a clear design methodology for the Engine Reservoir, to be followed for the first Engine Reservoir design but also flexible and well-detailed so that the design can be attractively optimised by reviewing the design steps. Accordingly, the problem statement is as follows:

Ocean Grazer company has a gap of knowledge on the Engine Reservoir requirements, on the main hydro-power machinery that must be contained inside and on the nature of the interactions with other Ocean Battery components and the environment. Consequently, the company is not able to develop a first design of the Engine Reservoir.

3 Design Scope

The problem identified in the previous section is of high dimensions. Therefore, a clear scope and boundaries of the design must be set, so that it is performed successfully and with the required quality.

3.1 System Description

Ocean Grazer company is currently working in two very different designs: the 'Buried' Design and the 'Suction Anchor-based' Design (Fig. 1). Although it is clear that its geometry is clearly different, they base on the same fundamentals: the energy storage through potential energy. The design project focuses on the design of the Engine Reservoir or Engine Room of the 'Buried' System.

The basic principle of the system is the following. There is a close circuit of fluid; the fluid can be stored in the Rigid Reservoir and in the Flexible Reservoir or Flexible Bladder, and both reservoirs are connected through a water conveyance system. The Rigid Reservoir is buried under the sea or lake soil (refered from here as seabed for the sake of briefty), and it contains both water and air in atomspheric pressure. That is to say, the Rigid Reservoir stored water is at atmospheric pressure. Contrarilly, the Flexible Reservoir is located on the seabed surface, and its flexible surface or bladder deforms without offering much resistance. Therefore, the Flexible Reservoir stored fluid feels the sea/lake hydrostatic pressure applied on the Bladder surfaces; the fluid is at the seabed hydrostatic pressure. Consequently, the fluid stored on the Flexible Reservoir has significantly more energy than the fluid stored on the Rigid Reservoir due to the height difference between reservoirs and due to the pressure increase described previously.

It has already been said that the Ocean Battery is to be implemented as a battery for renewable power plants. At a certain moment, it can be of interest of the power plant to store produced energy on the Ocean Battery. Then, the Ocean Battery stores this additional energy in the form of potential energy by pumping the fluid from the Rigid Reservoir (low energy fluid) to the Flexible Bladder (high energy fluid). Contrarily, the grid might demand energy at a certain moment, and then the Ocean Battery discharges by dropping the fluid from the Flexible Bladder to the Rigid Reservoir through a turbine. Therefore, the Engine Reservoir must contain all the hydro-power and electric components to store energy (battery charging) and to deliver energy (battery discharging).

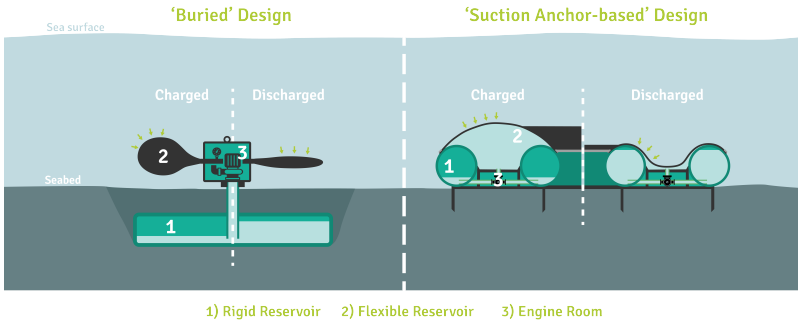

Figure 1: Scheme of the Ocean Battery current designs: the 'Buried' Design and the 'Suction Anchor-based' Design

3.2 Goal Statement

The goal statement is formulated from the problem statement (Section 2.1) and the system description (Section 3.1). From a general problem context of lack of a Engine Reservoir comprehensive design, the following goals have been defined:

- Identify the Engine Room or Reservoir design requirements
- Make a preliminary design of the hydropower components
- Clearly identify the main interactions between the Engine Reservoir and sea/lake, the seabed soil and the Rigid and Flexible Reservoirs.
- Elaborate a method for calculating the main loads derived from the identified interactions.
- Elaborate a first design and analyse its mechanical performance.

4 Methodology

As observable on the previous sections, the project encompass a high variety regarding the literature research and field of study. There is a important research work to be done on hydro-power components, which will conclude on a approximate layout of the components inside the Engine Reservoir. On the other side, there is research to be done on the behaviour of the seabed, the fluid and the solid structure, and the main loads that drive its interactions. This workload must be complemented with simulations and qualitative results, and it will conclude with the mechanical analysis of the design proposed in the first part of the project, and its evaluation. Accordingly, both the workload and the report are structure in two parts: 'Hydro-power components characterisation and Design description' and 'Engine Reservoir interactions characterisation and Mechanical analysis'.

4.1 Hydro-power components characterisation and Design description

The hydro-power components characterisation is the result of extensive literature research on the field of Pumped Storage Hydroelectricity or PHES. Some approximate calculations will be done as a function of the design variable d_{buried}, which refers to the Engine Reservoir base depth with respect to the seabed or soil surface (or the equivalent design variable H_d, introduced further in the report). It has been chosen to maintain d_{buried} as a variable for a significant part of the work in order to make the design method as general and flexible as possible, and to stress the significant effect of the buried depth in many stages of the design. Finally, some approximations and simplifications are made for the development of the first design of the Engine Reservoir by taking into account the system requirements and characterised hydro-power components.

4.2 Engine Reservoir interactions characterisation and Mechanical analysis

Firstly, a research work is done in the field of the interactions between the Engine Reservoir and the other Ocean Battery components (Rigid Reservoir and Flexible Bladder) and between the Engine Reservoir and the environment (Fluid and Soil domains). Following to the literature research, some simulation and analytical models are developed in order to quantify the interactions, and identify which of them are significant for the mechanical behaviour of the structure. Lastly, a comprehensive model of the Engine Reservoir that includes the significant interactions is simulated and evaluated.

Matlab software is used for some analytical calculations. When simulation tools are required, two Finite Element Method based softwares are used: COMSOL Multiphysics and CYPECAD.

4.2.1 COMSOL Multiphysics

COMSOL Multiphysics is a Finite Element Method solver that can simulate a bast quantity of physics phenomena. It is specialised on the following physics: electromagnetism, structural mechanics, acoustics, fluid flow, heat transfer and chemical engineering [**?**]. Through a user friendly interface, the physics governing equations are implemented through the description of the geometry, the material domains and the boundary conditions. It is used to model the fluid and structure basic behaviour, but the lack of the proper licences has difficulted the simulation of the soil behaviour.

4.2.2 CYPECAD

CYPECAD software is a Finite Element Method solver specialised on steel and concred reinforced structures. It carries an analysis and design of the structures, and it allows the application of horizontal and vertical forces on the project design [12]. It has been implemented to account for the steel reinforcement and in order to obtain a more complete mechanical analysis that COMSOL could not provide.

5 Design criteria and requirements

In order to develop the Engine Reservoir design, the design criteria and requirements must be clearly identified. They are defined in the following subsections.

5.1 Design criteria

The design considerations are guided by the philosophy of the so-called Limit State Design [23]. The design has to satisfy the following criteria:

- Ultimate Limit State (ULS): It requires the estimation of the maximum loads due to all possible design load cases, and comparing them with the load absortion capacity of the structure. The main loads taken into account are the overturning moment and the vertical and lateral loads. This consideration requires the computation of the ultimate moment and the lateral and axial load capacities. Therefore, ULS will provide an estimation of the the required minimum structure dimensions and shape. The ULS inputs are given by the location characteristics, such as the wave and current data. The earthquake and ice loads of extreme environmental conditions are out of the scope.
- Fatigue Limit State (FLS) and long term deformation: It requires the prediction of the fatigue life and the long term cyclic loading of the structure.
- Robustness and ease of installation: It determines whether the structure can be installed with the required redundancy.
- Functionality: It determines the purpose and actions of the Engine Reservoir, such as containing the necessary machinery for a Pumped-Storage Hydropower station and allowing the flow between flexible and rigid reservoirs. Functionality requirements are defined by the stakeholder Ocean Grazer.
- Compatibility: The design of the Engine Reservoir must be compatible with the design of the buried rigid reservoir/s and the flexible bladder/s that constitute the Ocean Battery system. The compatibility requirements are given by the stakeholder Ocean Grazer, and include the multiple connection between the Ocean Battery main components (Engine Reservoir, Flexible Bladder and Rigid Reservoir) and the required depth of each component.

The design requirement are summarised in Table 1 and related to design criteria described above.

5.2 Design Requirements

Requirement id.		Category	Description	Limit
R1	R1.A	ULS	The load carrying capacity of the Engine Room has to exceed the maximum possible loads. The considered loads are the lateral and vertical loads and the overturning moment.	$F_{h,ULS} < F_{h,ER}$ $F_{v,ULS} < F_{v,ER}$ $M_{ULS} < M_{ER}$
	R1.B	ULS	The Engine Room yield strength has to exceed the structure maximum stress.	$\sigma_m < f_{yk}$
R2	R3.A	SLS	The initial and accumulated deflection have to be less than 0.5m.	$\rho_0 < 0.5m$, $\rho_{acc} < 0.5m$
	R3.B	SLS	The initial and accumulated tilt have to be less than 0.5° and 0.25° respectively.	$\theta_0 < 0.5^{\circ}$, $\theta_{acc} < 0.25^{\circ}$
R3	R3.A	Functionality	The Engine Room must be isolated and contain air at atmospheric pressure	
	R3.B	Functionality	The Engine Room must contain the machinery for a pumped-storage hydropower.	
	R3.C	Functionality	The Engine Room machinery must ensure a production capacity of 1 to 2 MW with redundancy	$1MW < P < 2MW$
	R3.D	Functionality	The Ocean Battery must have a discharge time of 1/2 hour and a charging time of 2-4 hours.	$T_{discharge} = 0.5h$ $T_{charge} = 2h$
	R3.E	Functionality	The Engine Room must foresee future design modifications, such as an increase of the production capacity and of the number of reservoirs.	
	R3.F	Functionality	The Engine Room must allow maintenance and replacement operations	
R4	R4.A	Compatibility	The Engine Room must be connected to single/multiple flexible bladders through water flow inputs/outputs.	# connections: n_{FB} $z_{FB,connection} > z_{FB,bottom}$
	R4.B	Compatibility	The Engine Room must be connected to the single/multiple rigid reservoirs through water flow inputs/outputs.	# connections: n_{RR}
	R4.C	Compatibility	The Engine Room's pump must be located at a lowest height than the lowest water level of the rigid reservoir/s.	$z_{PT} < z_{RR,bottom}$

Table 1: Design criteria and requirements for the Engine Reservoir design

6 Design Input Data

Previous to the hydro-power components characterisation and the interaction loads analysis, the input data of the system must be defined. It refers to the environmental conditions as well as the system location under the water level. Initially, the Engine Reservoir had to be located in the sea environment, therefore data was collected for a specific location in the Northern sea where there is a wind-power plant. As the system has been finally decided to be located on a lake, the meteocean data (currents, waves and wind related data) has been considered of less importance for the project. Then, the collected data has been moved to Appendix A, to be consulted for further projects of Ocean Grazer in the sea environment.

6.0.1 Geological and Geotechnical data

The water depth considered is $d = 35m$, which corresponds to the mean water depth of the TNW wind farm zone [2]. For initial studies, the seabed is considered flat and of depth d. It is of high importance to perform a complete soil study for a project such as the Engine Room, as soil-structure interaction is highly dependent on soil properties. For instance, the skin friction is modelled differently for cohesive and non-cohesive soils (Section 9.1.2). Due to the fact that the Ocean Grazer has not yet decide on the exact location of the Engine Reservoir, there is no accurate data of the soil that interacts with the structure. Therefore, several types of soil are considered (Table 2,3), and its performance compared.

The maximum buried depth of $d_{buried,max} = 50m$ is provided by the stakeholder Ocean Grazer. This parameter refers to the maximum depth that the Engine Reservoir and the Rigid Reservoir can be buried below the mudline. The bigger the buried depth, the smaller flow rate is required for the same turbine power production. Nevertheless, the stress felt from the embedded structure walls and caused by the soil with depth. Therefore, the choice of the design variable $d_{buried} \in (0, 50)m$ is a compromise between the discharge flow (or generation power) and the strength of the structure.

7 Hydro-power components

The hydro-power components necessaries for satisfying the Engine Reservoir requirements of production and storage of energy are the same as the Pumped Hydropower Storage plants (PHES) [22]. They are described in Section 7.1 and characterised for the Engine Reservoir requirements in Section 7.2

7.1 PHES Main Components

The analogy with PHES is that the Flexible Bladder works as the 'upper reservoir', and the Rigid Reservoir as the 'lower reservoir'. The main components are briefly described below.

Headrace tunnel
Drives the fluid from the upper reservoir or Flexible Bladder to the penstock.

Penstock
Conduit for water flow between the upper reservoir (Flexible Bladders) and the turbine. Pipes are used for above-groud penstocks, and shaft or tunnels for below-ground cases. The typical flow velocity range is 1-5 m/s and typical diameter of 5-10 m. The cross-sectional area design is a trade off between cost and efficiency for a given flow rate Q: a large diameter provides a sower flow with lower losses but higher construction cost.

Surge tanks
Surge tanks of hydraulic bypass capacitors located on the penstock or on the tailrace. Their function is to absorb high pressure transients that might occur during startup or mode changeover.

Variable name	Symbol	Value			Unit
		Kaolin clay	Nkossa clay	Qiantang river silt clay	
Unified Soil Classification	USC	OH	CH	OH	[-]
Effective soil weight	γ'	6500	6000	8823	[N/m^3]
Internal angle of friction	ϕ	26	19	36.5	[º]
Adhesion factor	α	0.5	0.45	0.5	[-]
Soil cohesion	c	10	11	10	[kPa]
Mudline undrained shear strength	$c_{u,mud}$	4.0	5.0	6.0	[kPa]
Mudline undrained shear strength rate	m_{c_u}	1.50	1.67	1.35	[kPa/m]
Lateral earth pressure coefficient at-rest	K_0	0.562	0.674	0.405	[-]
Overburden bearing capacity	N_q	14.210	6.701	50.351	[-]
Self-weight bearing capacity	N_γ	12.624	4.693	61.390	[-]
Cohesion bearing capacity	N_c	27.085	16.558	66.695	[-]

Table 2: Soil parameters for cohesive soils: Kaolin clay, Nkossa clay and Qiantang river silt clay [18].

Variable name	Symbol	Value				Unit
		Silica sand	Statoil sand	Redhill 110 sand	Luce Bay sand	
Relative density	-	loose	very dense	loose	very dense	[-]
Effective soil weight	γ'	5993	8500	7820	10300	[N/m^3]
Internal angle of friction	ϕ	36	45	36	45	[º]
Limit unit end bearing	$q_{ult,lim}$	2.9	12.0	2.9	12.0	[MPa]
Limit unit skin friction	f_{lim}	67.0	114.8	67.0	114.8	[KPa]
Lateral earth pressure coefficient at-rest	K_0	0.412	0.293	0.412	0.293	[-]
Overburden bearing capacity	N_q	47.156	173.285	47.156	173.285	[-]
Self-weight bearing capacity	N_γ	56.655	271.717	56.655	271.717	[-]

Table 3: Soil parameters for cohesionless soils: Silica sand, Statoil sand, Redhill 110 sand and Luce Bay sand [18].

Draft tube:
Vertical conduit that drives the fluid from the turbine to the Tailrace tunnel.

Tailrace tunnel
Conduit for water flow between the pump and the lower reservoir (Rigid Reservoirs). Typically, they have lower pressure and flow rate than the penstocks, and therefore larger diameter. It is required a downward slope from the lower reservoir to the pump in order to create a pump inlet head that prevents cavitation in pumping operation.

Power house or Engine Reservoir
Contains the pump, turbines, motor and generators. It is typically located bellow the lower reservoir level so that there is the required inlet head for the pump. Three configurationts are possible for the power machines (Fig. 2), and its eligibility depends on the design requirements for efficiency, dimensions and cost:

- Quaternary set: on e pump, turbine, motor and generator. The pump and turbine are completely decoupled; the pump is driven by the motor and the generator is driven by the turbine. High efficiency is achieved as both the pump and turbine operate a its best efficiency conditions, but the equipment and infrastructure costs are notably higher than the other configurations.
- Ternary set: one turbine, one pump and one reversible motor/generator, all connected to the same shaft. Typically, the turbine is rigidly coupled to the reversible motor/generator, while the pump is coupled to the shared shaft with a clutch. High efficiencies are achieved, as the pump and turbine are optimised individually. Turbine and pump can operate simultaneously, and the turbine can also be used during pump startup to reduce the changeover time.
- Binary sets: one reversible pump/turbine (or pump working as a turbine) and one reversible motor/generator. It is the configuration with the lowest costs (simplified hydraulic pathways and less hydraulic and elecrical machines). Contrarily, it provides a lower efficiency than the other configurations as the reversible pump/turbine design is obtained as a compromise between the performance of the pump and the turbine. Additionally, the changeover time is larger than for other sets because the shaft and motor/generator have to change its rotational direction.

Nowadays, it is commonly used binary configuration on PHES applications due to the significant reduction of costs. Nevertheless, ternary configuration is used instead of binary configuration when the head and flow requirements exceed the operational ranges of the available reversible pump/turbines. Additionally, ternary configurations are also preferred for large PHES due to its higher efficiency.

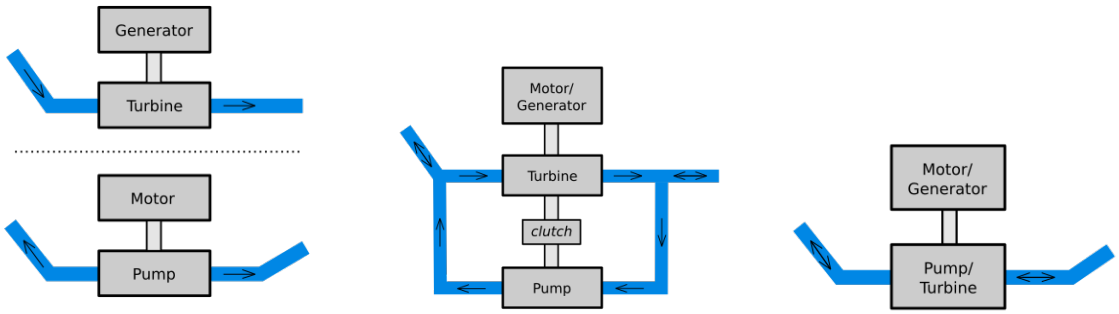

(a) (b) (c)

Figure 2: PHES configurations: (a) quaternary, (b) ternary, (c) binary

7.2 Hydro-power components characterisation

Requirement R5.B states that the Engine Reservoir must contain the main elements that characterise the powerhouse of a conventional pumped-storage hydropower station defined in the previous section. The Engine Reservoir machinery must allow the Ocean Battery to act as a battery (energy storage) and as a power station (energy generation). In order to do so, it must include the following elements: turbines, pumps, generators, motors, transformers, control system and ancillary rooms (electrical rooms, drainage gallery, cooling systems). Moreover, it is possible that the Engine Reservoir contains some elements for water conveyance, such as the penstocks and multiple steel gates and valves.

The scope of the design project only considers the Engine Reservoir elements that have a non-negligible influence on the mechanical study of the structure and the fulfilment of the requirements. For the equilibrium state and loads analysis, an approximated machinery weight is used, which is obtained from the selection of the heavy machinery (turbines, pumps, generators, motors, transformers). For the eigenfrequency analysis, a turbine and pump selection (following the requirement R5.C) is necessary to determine the operating frequency and to compare it with the structure natural frequency. The flow rate at the Engine Reservoir connections is extracted from the turbine selection.

According to the requirements and the project description, the structure must be fully underwater and half-buried on the seabed and it has to allow for an environment of atmospheric pressure inside. Therefore, the design intents to reduce as much as possible the dimensions of the Engine Reservoir, while still allowing redundancy and maintenance operations. Taking these requirements into consideration, reversible machine sets are eligible for the design, as they save both equipment and civil costs. In particular, it is required the use of reversible pump/turbines and reversible electric motor/generators. The reversible pump/turbines can work as a pump or as a turbine depending on the rotation direction. Every pump/turbine set is coupled to a reversible electric motor/generator, that works as a motor for the pump mode of the pump/turbine (storage operation of the Ocean Battery cycle) and as a generator for the turbine mode (electricity production operation of the Ocean Battery cycle).

7.2.1 Characterising the reversible pump/turbine

The main characteristics of a reversible pump/turbine are the output production, the best efficiency head, the turbine and pump operating head ranges, the impeller or runner diameter and the rotational speed. This characteristics will be approximated for the capacity production and redundancy requirements using the equations and relationships from [25].

The turbine head depends on the depth of the flexible bladder/s and the rigid reservoir/s. From the previous section 6.0.1, it is obtained a mudline depth of $z_{mudline} = 35m$ (**??**) and Rigid Reservoir and Engine Reservoir depth below the mudline of $d_{buried} \in (0, 50)m$. Accordingly, the total depth of the Rigid Reservoir is $z_{RR} = z_{mudline} + d_{buried} \in (35, 85)m$. For the case of the Flexible Bladder, it is clear that it must be located underwater and at the maximum depth possible (in order to maximise its energy storage capacity). From the previous argument, it is assumed the limit case of the flexible bladder located just above the mudline, at the maximum depth of $z_m udline$. The turbine best efficiency head is defined as the difference of hydraulic pressure between the flexible bladder and the flexible reservoir, in units of height of the water column. For the system considered, the pressure difference is caused by the water column above the flexible bladder (of height $z_{mudline}$) and the height difference between the flexible bladder and the rigid reservoir (d_{buried}). Therefore, the best efficiency head is given by $H_{BE} = z_{mudline} + d_{buried} \in (35, 85)m$. It should be noted that the effective head decreases as the rigid reservoir fills, but this consideration has been neglected for simplicity and because of the lack of a definitive design of the Rigid Reservoir.

The requirements state that the Engine Reservoir machinery must ensure a production capacity of 1 to 2MW with redundancy. It is decided to include 4 reversible pump/turbines of 0.5MW in

the design, so that the efficiency and redundancy criteria are satisfied. From Figure 3 and using the data of 0.5MW of power production capacity and $H_{BE} \in (35, 85)m$ of total differential head, the chosen reversible pump/turbine is of Francis type. For minimum $H_{BE} = 35m$ it is required a capacity of $Q_{t1} = 1.58\text{m}^3/\text{s}$ (turbine t_1 in Figure 3) and for maximum $H_{BE} = 85m$ it is obtained $0.1 < Q_{t2} < 1\text{m}^3/\text{s}$ (turbine t_2 in Figure 3).

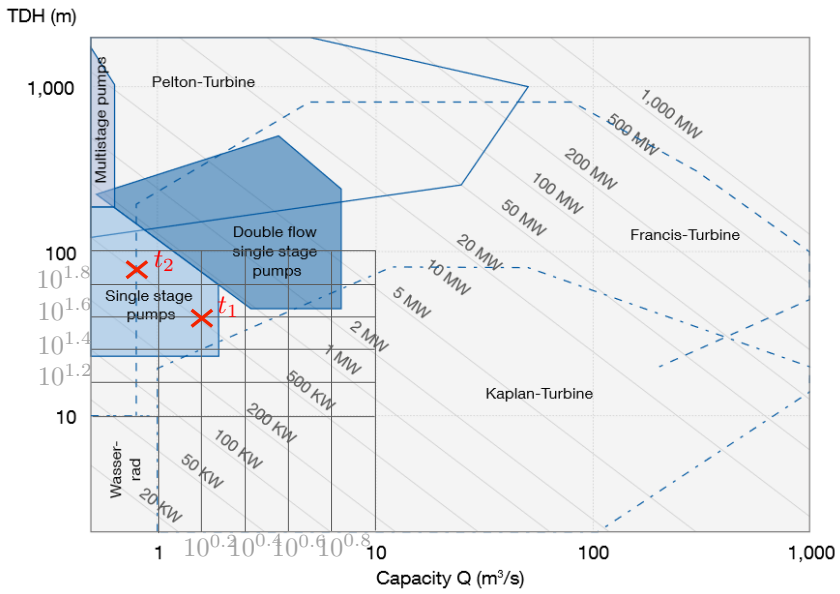

Figure 3: Schematic relationship between the power (grey isocurbes, in MW), the capacity (Q, in m^3/s), the total differential head (TDH, in m and logarithmic axis) and the turbine type (delimited regions) of a pump/turbine. The red cross corresponds to the chosen pump/turbine for the design. The original image has been taken from Sulzer public portfolio [33], and modified afterwards.

The velocity ratio ϕ_1 establishes the relationship between the rotational speed n (revolutions/min or r/min), the discharge diameter of the impeller D (m) and the best efficiency head H_{BE} (m) developed by the pump or absorbed by the turbine as:

$$\phi_1 = \frac{\pi n D}{(60[s/min])(2gH_{BE})^{1/2}} = \frac{(11.8 \cdot 10^{-3}[min/m^{1/2}])nD}{H_{BE}^{1/2}} (\text{metric}) \tag{1}$$

From Eq. 1, and choosing the design head H_d as the best efficiency head, it is direct to obtain the expression of the impeller/runner diameter:

$$D = \frac{\phi_1 H_d^{1/2}}{(11.8 \cdot 10^{-3}[min/m^{1/2}])n}, \tag{2}$$

Additionally, the available power (P) from the stored water in the flexible bladders is calculated from:

$$P = \rho Q_t g H_d \eta_t, \tag{3}$$

where $P = 0.5MW$ is the available power at full gate capacity, $\rho = 1000kg/m^3$ is the water density, Q_t is the water flow (m^3/s) of the reversible pump/turbine inlet when it operates in turbine mode (flow from the flexible bladder system), $g = 9.81m/s^2$ is the gravity acceleration, $H_d \in (35, 85)m$ is the designed head where best (peak) efficiency is obtained and $\eta_t = 0.80$ is the turbine efficiency. Finally, the turbine design specific speed (n_{st}) is given by:

$$n_{st} = \frac{n P_{KW}^{1/2}}{H_d^{5/4}}, \tag{4}$$

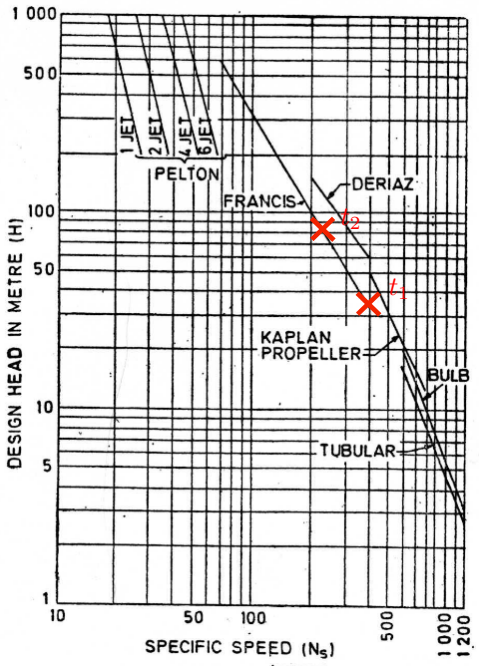

Figure 4: Relationship between Head (in meters) and Specific Speed (N_s or n_s) for diverse turbine types. The red cross corresponds to the chosen pump/turbine for the design. The original image has been taken from [30], and modified afterwards.

where n is the rotational speed in revolutions/min and $P_{KW} = 500KW$ is the turbine full-gate capacity in KW.

Substituting Eq. 3 for the chosen turbine parameters and the allowed range of design head values, it is obtained the water flow Q_t inversely proportional to the design head as $Q_t = 63.7105/H_d$. The result is shown in Fig. 6(a), and the limit values of the turbine capacity are $Q_{max} = Q_{t1}(H_d = 35m) = 1.82m^3/s$ and $Q_{min} = Q_{t2}(H_d = 85m) = 0.75m^3/s$. The capacity values match with the approximated data from Fig.3.

For the calculation of the rotational speed (n) using Eq. 4, it is first required to get an approximate expression of the turbine design specific speed for the case of the chosen Francis turbine. From Fig. 4, it is clear that the decimal logarithms of design head and specific speed are related linearly as:

$$\log_{10} n_s = m \log_{10} H_d + b, \tag{5}$$

where the fitting coefficients $m = -0.5857$ and $b = 3.4721$ are calculated using approximate data from Fig. 4. The resulting specific speed for the range of values of design head is shown in Fig. 6(b). Substituting Eq. 4 for the studied range of H_d, it is obtained the required rotational speed for a specific value of H_d. The result is shown in Fig. 6(c), and the limit values for the rotational speed are $n_{min} = n_{t1}(H_d = 35m) = 1407.5rev/min$ and $n_{max} = n_{t2}(H_d = 85m) = 2537.7rev/min$.

Similarly, the impeller/runner diameter expression (Eq. 2) is evaluated using the calculated values of rotational speed for every design head and the approximation $\phi_1 = 1$ for a pump/turbine working at the best effective head (for both turbine and pump operation modes). The resulting diameter as a function of design head is shown in Fig. 6(d). The figure shows small variation of the diameter for the whole range of allowed design head, with $D_{max} = D_{t1}(H_d = 35m) = 0.308m$ and $D_{max} = D_{t2}(H_d = 85m) = 0.356m$. This result implies that the turbine size (and weight) will be the same for all possible buried depths, but the capacity or flow rate and the rotation speed will change with the buried depth. For the weight calculation below it is used the mean value

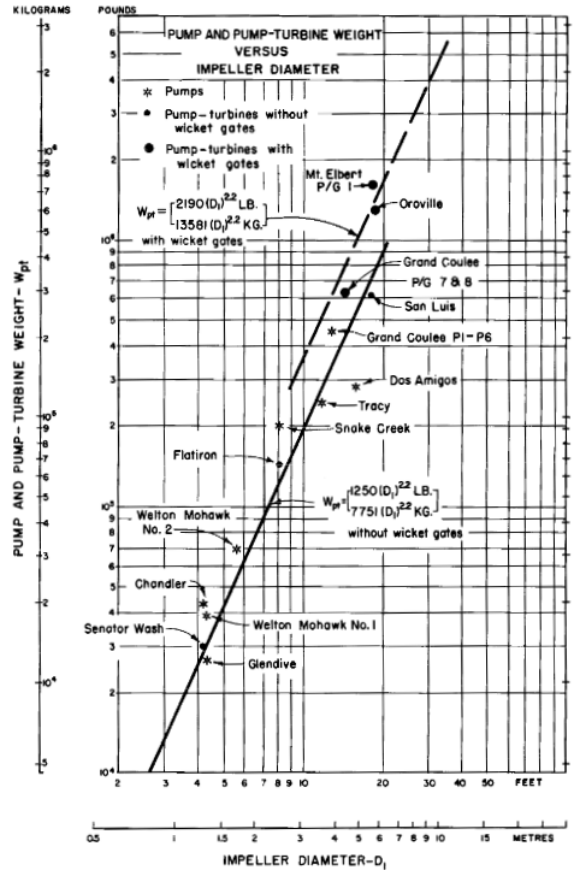

Figure 5: Turbine and pump/turbine weight versus the impeller diameter. Image obtained from [25]

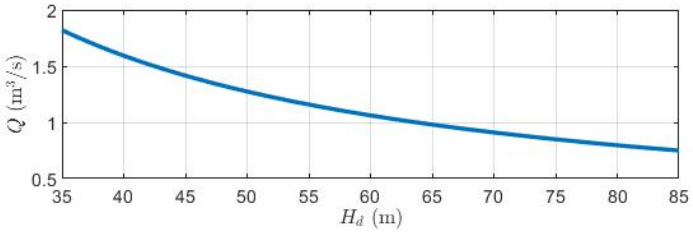

(a) Capacity or Discharge Flow (Q) as a function of Design Head (H_d)

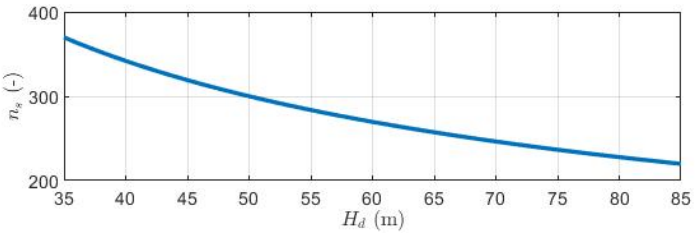

(b) Specific Speed (n_s) as a function of Design Head (H_d)

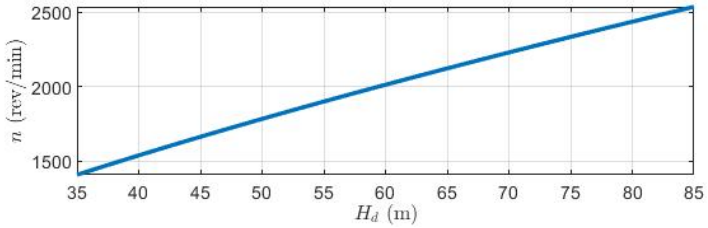

(c) Rotational Speed (n) as a function of Design Head (H_d)

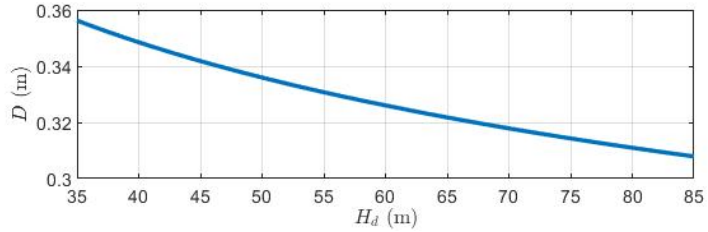

(d) Impeller/Runner Diameter (D) as a function of Design Head (H_d)

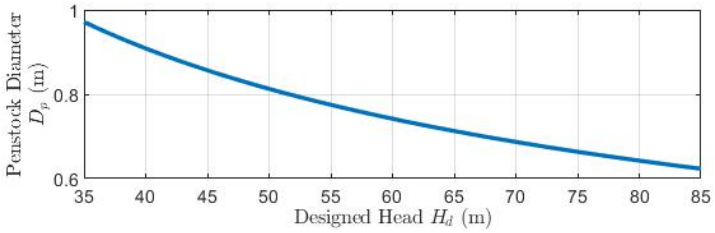

(e) Penstock Diameter (D_p) as a function of Design Head (H_d)

Figure 6: Calculated turbine and penstock design parameters for the studied range of values of the design head (H_d). The studies parameters are (a) Capacity or discharge flow, (b) Specific speed, (c) Rotational speed, (d) impeller/runner diameter and (e) penstock diameter.

$D = 0.332m$.

The weight approximate calculation is based on the data from Figure 5. It shows the relationship between the impeller diameter D and the pump and pump/turbine weight W_{pt}. Unfortunately, it has not been possible to find weight data for the small dimensions and production capacity of the design, as the existing pumped-storage facilities have notably bigger production capacity and consequently bigger impeller diameter for the reversible pump/turbines. Consequently, in order to determine the weight of the chosen reversible pump/turbine, it has been used the approximation that the relationship shown in Figure 5 for impeller diameter $D \in (0.5, 15)m$ is also true for the smaller diameter $D = 0.332m = 1.089ft$. Then, an approximate calculation of the reversible pump/turbine weight is obtained from the exponential regression of the figure (a continuous line in a log-log representation). Using the data from the figure, the linear regression for the log-log plot at the smallest range of impeller diameter (continuous line) can be written as:

$$\log_{10} W_{pt} = m \log_{10} D + b, \tag{6}$$

where the fitting coefficients $m = 2.193$ and $b = 3.047$ are calculated using Fig. 5 approximate data.Substituting m and b values in 6 for the calculated impeller/runner diameter of $D = 0.33m = 1.08feet$, it is obtained the reversible pump/turbine weight $W_{pt} =\simeq 1319pounds = 598kg \approx 600kg$.

7.2.2 Characterising the water conveyance system

The water conveyance system is composed by the following elements: water intakes (working as inlets and outlets), supply works, penstocks and tailraces [11]. The water intakes must be at the lowest point of the flexible reservoirs, and the water is conducted from the water intakes to the penstocks through the supply works or headraces. The penstocks are the conduits or pipes that bring the water from the intakes or the supply works to the reversible turbine-pump overcoming the head difference. They are usually made of steel, and they must ensure high pressure on the inside in case there are sudden load increases or decreases. Finally, the tailrace connects the reversible pump/turbine to the rigid reservoir.

The penstocks diameter is of special interest for the Engine Reservoir design, as it should be taken into consideration for the estimation of the Engine Reservoir dimensions. Although the flexible bladder intake and supply work is out of the scope of the project, it is worth mentioning that typically every reversible pump/turbine has its own penstock, but the multiple penstocks may or may not share the same water intake or supply channel. The penstock diameter (D_p) is directly related to the penstock rated discharge (Q_D), which coincides with the turbine mode inlet flow (Q_t) calculated in Eq. 3. The optimum diameter for small hydropower projects and as a function of the rated discharge was developed by Warnick et al. (1984) as:

$$D_p = 0.72\sqrt{Q_D} \tag{7}$$

Substituting $Q_D = Q_t$ in the previous expression and using the relationship between the turbine flow rate with the design head (Eq. 3, the penstock diameter is calculated as:

$$D_p = 0.72\sqrt{\frac{P}{\rho g H_d \eta_t}} \propto H_d^{-0.5} \tag{8}$$

The optimum D_p for the available range of H_d is shown in Fig. 6(e); it decays with H_d as $H_d^{-0.5}$. Then, the maximum value of $Q_{p,max} = 0.97m$ is obtained for minimum design head $H_d = 35m$, and the maximum $Q_{p,min} = 0.62m$ is obtained for maximum $H_d = 85m$. From this result and the requirement of being able to install up to 4 reversible pump/turbines of 500KW, it is obtained an additional requirement for the Engine Reservoir: The Engine Reservoir has to allow the installation of up to 4 steel penstocks of diameter $D_p \in (D_{p,min}, D_{p,min})$ which will depend on the buried depth of the structure.

Additionally, an estimate weight computation can be made for more accuracy in loads calculation. It is used that the penstock is made of steel, as it is common for small hydropower projects. In addition, it is used a totally vertical penstock to minimise its length and the Engine Reservoir dimensions. Then, the penstock length corresponds to the height difference between the flexible bladder intake and the pump/turbine bladders. Using the assumption that the flexible bladder intake must be near the seabed, the penstock length is approximately $L_p \simeq d_{buried} \in (0, 50)m$. The maximum penstock weight ($W_{penstock}$, [N]) is found when it is full of water:

$$W_{penstock} = \left[\frac{\pi D_p^2}{4} \rho_w + \frac{\pi}{4}((D_p + e)^2 - D_p^2)\rho_{steel} \right] g d_{buried} \tag{9}$$

The penstock wall thickness (e, in m) is calculated as [6]:

$$e = \frac{p_{total} D_p}{2\sigma_{steel}} \tag{10}$$

where p (Pa) is the total internal pressure within the conduit, D_p (m) is the outside diameter of the penstock, and σ_{steel} is the allowable tensile stress of the steel. The total internal pressure is caused by the static pressure (p) and the water hammer (p_h):

$$p_{total} = p + p_h \tag{11}$$

The maximum value of the static pressure p is found at the bottom of the penstock, and is given by $p = \rho_w g(z_{mudline} + d_{buried}) \in (0.34, 8.33)MPa$. Additionally, the water hammer appears when the turbine vale is closed, the flow stops abruptly and the dynamic energy is converted into elastic energy of pressure waves that travel back and forth the penstock (they are damped out due to friction). The velocity of the pressure wave in the penstock (c_p) can be approximated as $p_h = 0.20p$ for practical purposes [6]. Then, the internal pressure range for the range of admitted d_{buried} is $p_{total} = 1.2p \in (0.41, 10.0)MPa$ [19].

For normal conditions (earthquakes and penstock filling and draining not considered), the recommended allowable tensile stress is the smallest value between 2/3 the minimum yield stress and 1/3 the minimum tensile strength of the steel. Carbon steel (JIS SS400) is found to be used in the penstocks from hydroelectric power plants [16]. With $\sigma_y = 235MPa$ as minimum yield stress and $\sigma_t = 400MPa$ as minimum tensile strength [32], the penstock allowable stress is $\sigma_{steel} = min(2/3 \cdot \sigma_y, 1/3 \cdot \sigma_t) = 133.33MPa$.

Penstock thickness (e) is calculated substituting the previous values in Eq. 10. For the limit case of Engine Reservoir and Rigid Reservoir buried $d_{buried} = 50m$ below the mudline, it is obtained a maximum penstock thickness of $e = 23.25mm$.

The maximum penstock weight is approximately calculated for the maximum value of the design variables: $D_p = 0.97m$ and $e = 0.023m$. Substituting these values and carbon steel density of $\rho_{steel} = 7850kg/m^3$ in Eq. 9, it is obtained that the penstock weight ($W_{penstock}(d_{buried})$) will not exceed the limit of $W_{penstock}(d_{buried}) \leq 9.98 \cdot 10^3 d_{buried} < 10^4 d_{buried} \quad [N]$.

7.2.3 Characterising the reservoirs capacity

Reservoirs capacity refers to the maximum water capacity of the system of (multiple) Flexible Bladders and (multiple) Rigid Reservoirs. For simplicity, it has been assumed the same capacity for both the system of Flexible Bladders and Rigid Reservoirs ($C_{FB} = C_{RR} = C_{reservoirs}$). The water capacity of the reservoirs (Rigid Reservoirs and Flexible Bladders) depends on the power production ($1 < P < 2MW$, from Requirement R5.C), the discharge time ($T_{discharge} = 0.5h$, from Requirement R5.D), the turbines design head ($35m < H_d < 85m$, from Section 7.2.1) and the turbines discharge flow for a certain power production and turbine design head ($Q_{t1} = 1.82m^3/s$ for $P = 0.5MW$ and $H_d = 35m$ and $Q_{t2} = 0.75m^3/s$ for $P = 0.5MW$ and $H_d = 85m$, from Section 7.2.1).

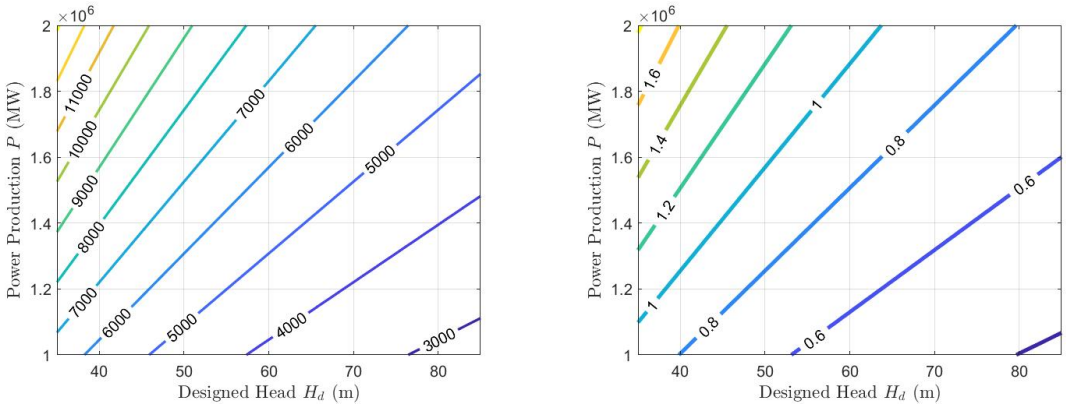

(a) Reservoirs Capacity, $C_{reservoirs}(m^3)$

(b) Pumping flow rate, Q_p (m^3/s)

Figure 7: Estimation of (a) Reservoirs Capacity and (b) Pumping flow rate for the studied value ranges of power production and turbine design head.

From the turbine power expression (Eq.3) and using the relationship between energy and power, it is obtained:

$$E_{discharge} = \int_0^{T_{discharge}} Pdt = \int_0^{T_{discharge}} \rho_w C_{reservoirs} g H(t) \eta_t(H(t)) dt \approx \tag{12}$$

$$\approx \rho_w C_{reservoirs} g H_d \eta_t \tag{13}$$

Secondly, the total energy produced by the complete discharge of the flexible reservoirs can be approximately calculated as:

$$E_{discharge} \approx P T_{discharge}, \tag{14}$$

where $C_{reservoirs}$ is the total capacity of the system of flexible reservoirs in units of volume of water (m^3 of water). This expression uses the approximation that the turbine efficiency ($\eta_t(H)$) and turbine head ($H(t)$) are constant through all discharge operation, and that the turbine head is equal to the design head (H_d). The approximation has been used due to the lack of information about the number of reservoirs and its shape and allowable water levels, which would provide the evolution of $H(t)$ during discharge, and the its corresponding $\eta_t(H)$. Combining Eq. 13 and 14 it is obtained the expression for the total water capacity of the (multiple) flexible bladders:

$$C_{reservoirs} = \frac{P T_{discharge}}{\rho_w g H_d \eta_t} \tag{15}$$

where $T_{discharge}$, ρ_w, g and η_t are known parameters. It is clear to see that that the volume capacity is directly proportional to the power production, and inversely proportional to the design head. Fig. 7(a) visualises the result of the $C_{reservoirs}$ calculation using Eq. 15 and range of values $P \in (1, 2)MW$ and $H_d \in (35, 85)$ aforementioned.

7.2.4 Characterising the pump flow rate

The pump characteristics derive from the reservoirs volume and desired pumping period. Then, the pumping period (T_{charge}) refers to the total time required to pump the water from the system of Rigid Reservoirs in its full capacity to the system of Flexible Bladders, initially in its minimum capacity. Assuming a constant flow rate for the whole pumping process for simplicity, it is direct to obtain that the pumping flow rate (Q_p) depends on the reservoirs volume and pumping or charging period as:

$$Q_p = \frac{C_{reservoirs}}{T_{charge}} \tag{16}$$

The pumping flow is calculated substituting the previous expression for the total volume of reservoirs ($C_{reservoirs}$ from Eq. 15) and the required charging time ($T_{charge} = 2h$, from Requirement R5.D). The pumping flow rate (Q_p) is calculated analogously as the reservoirs capacity ($C_{reservoirs}$) in the previous section; it is considered the aforementioned range of values for the design head (H_d) and power production (P). The results are shown in Fig. 7(b), where it is observed that the required pumping flow rate increases with power production and decreases with design head. The minimum and maximum values of the pumping flow rate are $0.4\text{m}^3/\text{s}$ and $1.8\text{m}^3/\text{s}$ for the studied range of P and H_d.

Estimating Motor/Generator Characteristics

Typically, the motor/generator is installed in vertical configuration above the turbine runner for vertical shaft turbines, and in horizontal configuration for horizontal shaft Francis turbines. For fixed-speed pump/turbine, it is required a synchronous motor/generator that works at a fixed speed in generating and pumping modes. It rotates synchronously with the AC grid frequency and it is excited with DC current (thyristor AC/DC converter required). For variable-speed pump/turbines, it is used a motor/generator with adjustable rotational speed. There are two types of adjustable rotational speed motor/generators: a synchronous motor/generator with variable speed or singly-fed and a doubly-fed asynchronous machine or DFAM [22]. While the DFAM configuration is preferred for large PHES ($> 100MW$), synchronous motor/generator with air/water cooling system in a closed circuit is chosen for the current design taking as a reference the Pre-Feasibility Study of Suduroy in Faroe Islands realised by Norconstult's [24].

Lots of difficulties have been encountered for the weight and dimension calculations for the generator and the motor, as manufacturing business do not share detailed information about their products. An approximate data of $m = 1320kg$ has been found for a 250kW wind-driven generator[31]. Due to the lack of more available data, the conservative and approximate calculation of $m = 3000kg$ is made for the motor/generator weight of the Engine Reservoir. No valuable information about the generator and motor dimensions have been found, just what is intuitive from the generators images. From this qualitative information source, the dimensions are set as 2m x 1m x 1m, to be review when more data is available.

8 Elaboration of the design geometry and material

The design geometry selection is made from the literature research and components characterisation of Section 7. As for the material selection, Ocean Grazer experience suggested that the Engine Reservoir should be made out of reinforced concrete.

8.1 Characterising the Engine Reservoir walls: thickness and reinforcement

An initial guess of the wall thickness and % of steel reinforcement is required to analyse the mechanical behaviour of the Engine Reservoir. These properties will be optimised afterwards from the results analysis in order to satisfy the strength requirements of the structure.

Wall thickness is taken from literature on structures with similar environment. It is taken wall thickness $t = 0.9m$ from the research on the design of a submerged floating tunnel [17], as it is subjected to strong hydrostatic pressures as the Engine Reservoir.

Regarding the walls reinforcement ratio, it is used the approximate data from Tab. 4. It is expected to obtain higher ratios in further steps of the design, as the Engine Reservoir must withstand significantly large hydrostatic and earth pressures.

Concrete Building Element	Weight of reinforcement (kg/m^3)
Bases	90-130
Beams	150 - 300
Columns	200 - 450
Footings	70 - 100
Retaining walls	110 - 150
Slabs	75 - 135

Table 4: Rule thumb of weight of steel reinforcement per cubic meter of concrete of different concrete building elements [29].

8.2 Design I

Following the requirements, the design must contain the elements drawn in Figure 8 and described belows:

- Reversible pump/turbines (1) and reversible motor/generators (2) connected through a vertical shaft (3): meets the requirements of energy production and storage.
- Penstocks (4): must be inside the Engine Reservoir for better protection to environmental loads and corrosion and to make possible future design modifications (add penstocks or change penstock diameter for bigger discharge flow).
- $n_{connection_{RR}}$ flow connections with the rigid reservoirs (5) and $n_{connection_{FR}}$ connections to the flexible bladders (6): the Engine Reservoir shape allows the addition of more connections to meet the requirement of future modifications.
- Machine Hall (7): it is defined as the Engine Reservoir area where the power machines are installed. It satisfies the requirement of production capacity as it stores the power machines. It also meets the requirement of the lowest high of the pump with respect to the Rigid Reservoir due to the fact that the Machine Room is buried into the sea bed at a lowest level than the RR.

- Engine Reservoir Shaft (8): it is defined as the Engine Reservoir area that overcomes the head difference between the Machine Hall and the Flexible Bladders. It must contain the penstocks and the $n_{connections,FB}$ to the flexible bladders (and guarantee the possibility of adding more flow intakes). Its sectional area must guarantee the machine/operators transport along the shaft for the requirement of maintenance and replacement operations.
- Exchange Zone (9): it is defined as the most upper zone of the Engine Reservoir. It is added to the design to meet the requirement of maintenance and replacement operations. It should be possible to change the medium of the chamber without altering the medium of the other Engine Reservoir zones. That is to say, it should be possible to change the Exchange Zone medium from air at atmospheric pressure to seawater when machines/operators are introduced into the Engine Reservoir, and then remove the sea water and recover the air atmosphere to then introduce the machines/operators into the Engine Reservoir Shaft and Machine Hall (and vice-versa). For the design project, it is also considered as an additional height of the Shaft, the medium change operations are out of the scope of the project.

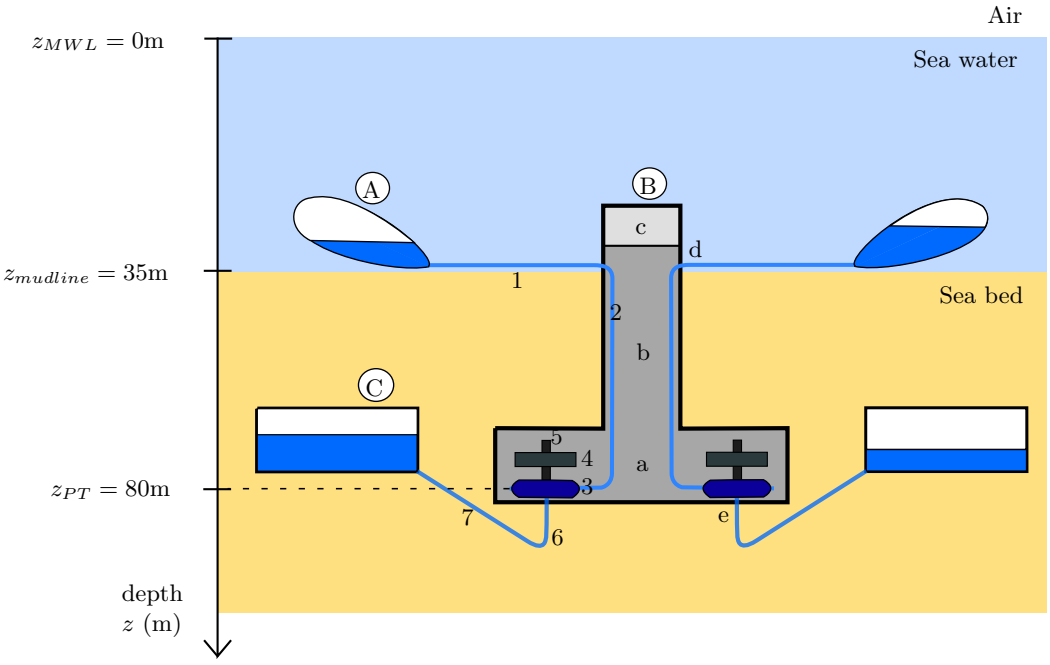

Figure 8: Lateral view of the initial shape and structure of the Engine Reservoir. The Ocean Battery main systems are itemised using letters: the Flexible Bladders (A), the Engine Reservoir (B) and the Rigid Reservoirs (C). The main components relevant for the requirements satisfaction and for the mechanical analysis are numbered (1-9).

Design variables are defined in Table 5, and shown schematic in the lateral view from Fig. 9. As observed in the table, it is chosen that both the Shaft and the Machine Hall have a cylindrical shape. This decision is based on the higher simplicity of the modelling due to the axial symmetry, and it does not interfere with any requirement. Other geometries are considered in Design II.

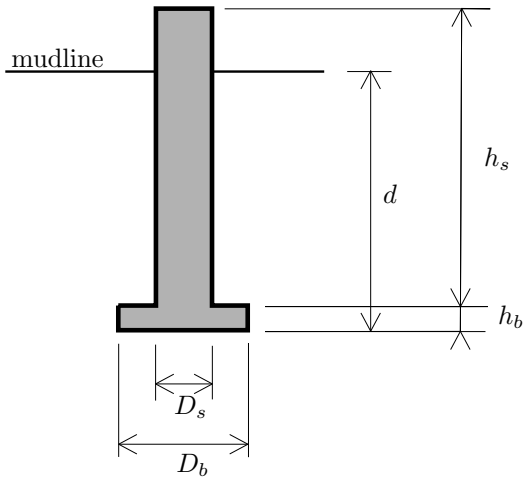

Figure 9: Schematic lateral view of some initial design variables of the Engine Reservoir.

Design variable	Symbol	Value	Unit
Engine Room embedded depth	d	50	m
Concrete steel reinforcement percentage	p_{sr}	5	%
Shaft shape	-	cylindrical	-
Shaft diameter	D_s	10	m
Shaft height	h_s	45	m
Shaft wall thickness	t_s	1	m
Shaft top covering thickness	t_{top}	2	m
Machine Hall shape	-	cylindrical	-
Machine Hall diameter	D_b	15	m
Machine Hall height	h_b	10	m
Machine Hall wall thickness	t_b	1	m
Machine Hall base thickness	t_{base}	2	m

Table 5: Initial values of the Engine Reservoir design variables.

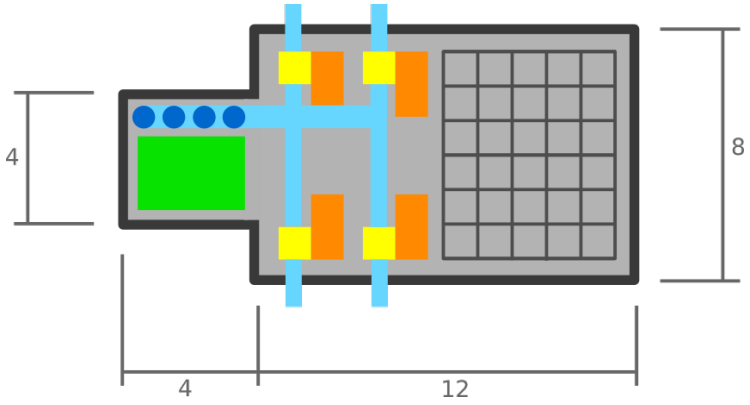

Figure 10: Top view of the Machine Hall, with the schematic distribution of the main Engine Reservoir in colours. The hydraulic and electrical components detailed are: pump/turbine (yellow), motor/generator (orange), penstocks (dark blue), water conveyance system except penstock (light blue), shaft elevator (green) and additional area for transformers, control system and other other ancillary rooms (gridded region).

8.3 Design II

Due to the difficulty of relating the dimension requirements that derive from the hydro-power components characterisation (Section 7.2) on a circular area and the foreseen difficulties on designing wall reinforcements for a cylindrical shape, a second design has been constructed, and considered in most of the models constructed in further sections. The 5 zones described in Design I are mantained in Design II.

Using the results from Section 7.2 on the main hydro-power machines, a Machine Hall distribution has been developed (Fig. 10). Significant amount of additional space has been left for the non-characterised componends of the Engine Reservoir (additional area for transformers, control system and other other ancillary rooms), indicated as a gridded region in the figure. Therefore, the design of the Machines Hall is to be optimised when more machine data is available.

The height of the structure is maintained as a design variable depending on the embedded depth. As the Exchange Room must be above the seabed, as well as the flow connections with the Flexible Bladders, the shaft continues above the seabed for additional $2m$ to account for the flow connections with the Flexible Bladder (Requirement R4.A), and the Exchange Room is designed of the same surface as the shaft (for simplicity purposes) and of $3m$ of height (enough to fulfill the Requirements R3.E and R3.F). In conclusion, the squared 4m x 4m that constituted the shaft and the Exchange Room reaches a height of $5m$ above the seabed, and the shaft length in the vertical axis will be given by the structure embedded depth.

9 Literature research: Engine Reservoir interaction loads

According to the requirements in Tab. 1 and the designs description in Section 8.2,8.3, the Engine Reservoir interacts with other Ocean Battery components (Rigid Reservoir, Flexible Bladders) and with its environment (fluid and seabed). This interactions, as all physical interactions, are two-way interactions or fully coupled interactions. In order to exemplify the concept, it is considered a fluid flow (component 1) and a flexible structure (component 2) located in a certain way that opposes the fluid flow. Then, the fluid flow exerts a load on the flexible structure (interaction 1→2), and as a consequence the structure suffers a displacement (result of interaction 1→2). But, at the same time, the structure displacement on the fluid domain causes a change on the fluid boundaries (interaction 2→1) which results in a change on the velocity field (result of interaction 2→1). It is now clear that any interaction or action implies a second interaction or reaction. The nature of this relations for the Engine Reservoir are detailed in Fig. 11.

It should be noted from the figure scheme that not all the interactions are described, but some interactions are studied as one-way interactions: from the Fluid to the Engine Reservoir, from the Fluid to the Seabed and from the Seabed to the Engine Reservoir. The fully coupled interactions found in the real case are simplified as one-way interactions. At this point of the argument, it is worth mentioning that the purpose of the interactions study is not to fully characterise the 3 domains (fluid, seabed and structure) but to obtain the boundary loads on the Engine Reservoir caused by the fluid. That is to say, the changes in the Fluid and Seabed are not of significance if they do not cause, at the same time, a significant change on the Engine Reservoir boundary conditions. Taking the example of Fluid - Engine Reservoir interaction, the one-way interaction from the fluid to the Engine Reservoir will cause small displacements and a stress distribution to the Engine Reservoir. Nevertheless, the effect that this changes will cause to the fluid are significantly small (slight change of the velocity field and pressures) and the interaction that this small changes in the fluid will cause to the Engine Reservoir are completely neglected. Therefore, one-way interactions are considered because an accurate modelling is only required for the Engine Reservoir domain.

According to the previous considerations, the design project and this Section will only describe the one-way interactions shown in Fig. 11. Before the interactions study, the stability conditions will be introduced for the vertical axis, which considers interactions between all Fluid, Seabed and Structure domains.

9.1 Stability conditions: uplift and driving

The aim of this section is to get an expression of the stability conditions for the phenomena of uplift and driving. Uplift phenomena refers to the structure rising due to buoyancy forces predominance. In contrast, driving phenomena describes the structure sinking due to gravity forces predominance. Therefore, stability in vertical direction is only reached if both uplift and driving conditions are satisfied. For the stability conditions analysis, it is required the previous calculation of the vertical deadweight of the structure and of the geotechnical load carrying capacities or resistances.

9.1.1 Structure vertical deadweight

First the vertical deadweight load of the structure must be calculated. The total vertical load of the structure is $W_T = mg$, where m is the total self-weight of the Engine Reservoir design. It accounts for the structural concrete weight (W_c),the walls steel reinforcement (W_{sr}) and the machinery weight (W_m). From the listed weights contribution, the calculation of the total structure self is given by:

$$W_T = W_c + W_{sr} + W_m \tag{17}$$

It might be necessary to consider an additional deadweight force, the soil filling weight (W_s). If applicable, its exact expression has to be determined from the structure shape and soil properties.

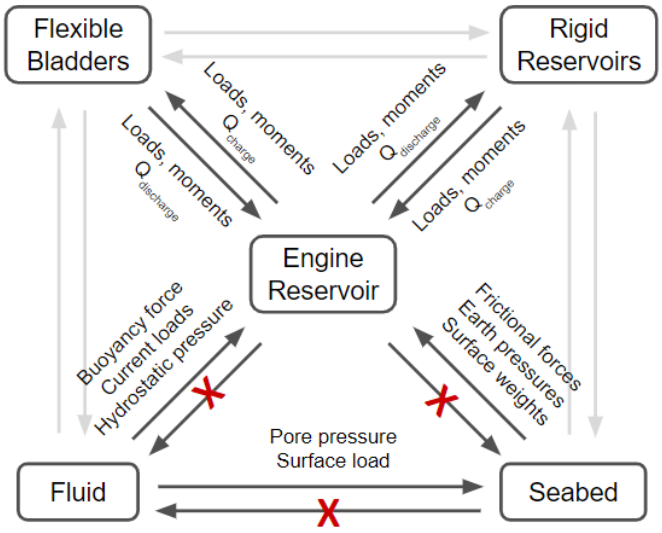

Figure 11: Scheme on the interactions between the Engine Reservoir, the other Ocean Battery main components (Flexible Bladders, Rigid Reservoirs) and the medium domains in direct contact to the Engine Reservoir (fluid and seabed soil).

It should be noted that the soil filling weight already considers the buoyancy effect (as the seabed mudline is bellow the water level or water top). Accordingly, W_S is calculated as:

$$W_S = \gamma_s V_s g - \gamma_w V_s g = \gamma' V_s g, \tag{18}$$

where V_s is the volume of the soil filling (m^3), γ_s is the dry soil density (kg/m^3), γ_w is the seawater density (kg/m^3) and γ' is the so-called effective soil density (kg/m^3).

9.1.2 Geotechnical load carrying capacity

The lateral and vertical load capacity of the structure must be calculated for both cohesive and cohesionless soils and compared with the applied loads as stated in the requirements. The load carrying capacity of vertical and partially embedded piles with closed end (plugged) has been studied in detail on the field of foundation structures, and its principles are applicable to the cylindrical design of the submerged and half-buried Engine Reservoir. In particular, the theory and expressions presented along the section are extracted from [1].

The ultimate bearing capacity for axial loading (Q_d, N), also referred as soil resistance to driving or compression ($R_{s,driving}$) is determined by:

$$R_{s,driving} = Q_d = Q_f + Q_b, \tag{19}$$

where Q_f is the skin or sliding friction resistance (N), Q_p is the total end bearing resistance(N). Following this definition, the soil resistance against uplift (due to buoyancy and added loads) is defined as:

$$R_{s,uplift} = Q_f. \tag{20}$$

The skin friction resistance (Q_f, N) is calculated through the integration of the unit skin friction capacity (f, Pa) along the side surface area (A_s, m^2) as:

$$Q_f = \int_{A_s} f(d) dS. \tag{21}$$

The integration over the surface is necessary due to depth dependency of the unit skin friction capacity ($f = f(d)$). The different expressions for the unit skin friction capacity are presented

bellow for cohesive and cohesionless soils (Eq. 29,32.

The end bearing capacity or resistance (Q_b, N) it typically calculated through ultimate Terzaghi's bearing capacity (q_{ult}, Pa) as:

$$Q_b = q_{ult} A_b, \tag{22}$$

where A_b is the base or footing area (m^2). Terzaghi's bearing capacity q_{ult} is the ultimate bearing capacity of the structure, that is to say, the smallest bearing load that causes the structure to fail. Then, it might be considered as the maximum bearing capacity, to which a factor of safety will be applied afterwards (Section 9.1). Terzaghi's bearing capacity formulation bases on the assumption that there is a triangle of pressure just bellow the base of the structure with angle between the base and the pressure triangle of $(45+\phi/s)$. Terzaghi's bearing capacity considers that the bearing capacity is developed due to the soil properties of cohesion, friction an density, and it is expressed as [28]:

$$q_{ult} = \underbrace{cN_c s_c}_{\text{cohesion}} + \underbrace{qN_q}_{\text{subcharge}} + \underbrace{0.5BN_\gamma \gamma' s_\gamma}_{\text{density}}, \tag{23}$$

The cohesion term ($cN_c s$) represents the strength due to cohesion, where c is the soil cohesion ($c = 0$ for cohesionless soils), N_c is the Terzagui's cohesion bearing capacity factor (obtained as Eq. 24) and s_c is the Terzaghi's cohesion shape factor (obtained from Tab. 6). The subcharge term (qN_q) refers to the bearing capacity strength due to the load subcharge exerted as added pressure by the soil above the structure base. The variable q is the effective stress at the structure base or footing (Eq. 28) and N_q is the Terzaghi's overburden bearing capacity factor (obtained as Eq. 25). Finally, the density term ($0.5BN_\gamma \gamma s_\gamma$) represents the strength due to soil density, where B is the base width or shorter dimension, N_γ is the Terzaghi's self-weight bearing capacity factor (obtained as Eq. 26), γ' is the effective soil density and s_γ is the Terzaghi's density shape factor (obtained from Tab. 6).

Terzaghi's bearing capacity factors N_c, N_q and N_γ are given as a function with respect to the internal friction angle of the soil (ϕ, in degrees) [9][13]:

$$N_c = \frac{N_q - 1}{\tan\phi} \tag{24}$$

$$N_q = \frac{e^{2\pi(0.75-(\phi/360))\tan(\phi)}}{2\cos^2(45+(\phi/2))} \tag{25}$$

$$N_\gamma = \frac{2(N_q+1)\tan(\phi)}{1+0.4\sin(4\phi)} \tag{26}$$

It should be noted that the factor N_c must not be calculated for cohesionless soils, as they have null soil cohesion per definition ($c = 0$ for cohesionless soils).

p_0 (Pa) is defined as the effective stress for a specific depth h, and it increases linearly with depth as:

$$p_0 = \gamma' h, \tag{27}$$

Substituting h for the depth of the structure base or footing (d) in the previous equation, it is obtained the effective stress at the structure base or footing (q, Pa):

$$q = \gamma' d, \tag{28}$$

where, as expected, q increases linearly with the depth of the structure base or footing, also referred as embedded depth.

A. Skin friction and end bearing in cohesive soils

The unit skin friction capacity (f, in Pa) for the case of cohesive soils is calculated through α-Method or Tomlinson Method as [27]:

$$f = \alpha c_u, \tag{29}$$

Terzaghi's Shape Factors	s_c	s_γ
Square footing	1.3	0.8
Strip footing	1.0	1.0
Round footing	1.3	0.6

Table 6: Terzagui's shape factors [28]

where α (dimensionless) is the empirical adhesion coefficient that reduces the average undrained shear strength c_u (Pa). The constrained factor $\alpha \leq 1$ may be computed as:

$$\alpha = f(\psi) = \begin{cases} 0.5\psi^{-0.5} & \text{for} \quad \psi \leq 1 \\ 0.5\psi^{-0.25} & \text{for} \quad \psi > 1 \end{cases} \tag{30}$$

where the local variable $\psi = c_u/p_0$ is a function of the averaged undrained shear stress (c_u) and the effective overburden pressure at a specific point (p_0, defined in Eq. 27).

The undrained shear strength calculation is complex, and diverse models have been developed for different types of cohesive soils from experimental measurements. For a more realistic calculation of c_u, the undrained shear strength data is obtained for different cohesive soils (Tab. **??**). In particular, the table provides the undrained shear strength at mudline ($c_{u,mud}$) and the rate of change of undrained shear strength with depth (m_{c_u}). Then, the averaged undrained shear strength from mudline to embedded depth d can be calculated as:

$$c_u = c_{u,mud} + \frac{m_{c_u} d}{2} \tag{31}$$

B. Skin friction and end bearing in cohesionless soils

For cohesionless soils, the unit skin friction capacity (Pa) is calculated as:

$$f = K p_o \tan\delta, \tag{32}$$

where K is the coefficient of lateral earth pressure and represents the ratio of horizontal to vertical normal effective stress, p_0 (Pa) is the effective overburden pressure at a specific point (defined in Eq. 27) and δ is the friction angle between the soil and the structure wall (degrees). The Engine Reservoir has a closed base, therefore it is studied as a plugged case and $K = 1$ is assumed. If no detailed measurements are available, ϕ may be selected from Tab. 2.

C. Skin friction and end bearing limitation in cohesive and cohesionless soils

It is direct to see from Eq. 32, that f increases linearly with the overburden pressure p_0, which increases linearly with embedded depth (Eq.27). Nevertheless, experimental data show that the skin friction do not increase indefinitely with depth; it reaches its peak value slightly above the tip, and is notably reduced after that. There is no satisfactory theory to analytically predict the nonlinear behaviour of the skin friction with depth, therefore engineers use the approximate theory of critical depth instead [34]. It states that the unit skin friction capacity f should be limited by a specific value f_{lim}. Following this argument, the expression of skin friction capacity (Eq. 32) is modified as:

$$f(d) = \begin{cases} K\gamma' d \tan\delta & \text{for} \quad d \leq d_{lim} \\ f_{lim} & \text{for} \quad d > d_{lim} \end{cases} \tag{33}$$

where d_{lim} is the limiting or critical depth from where the skin friction capacity is limited. As for the case of unit skin friction, it is also recommended to limit the unit end bearing value so that it does not infinitely increase with depth as the experimental data suggests. There is no valid theory for the end bearing capacity behaviour with respect to depth, therefore the critical depths defined for skin friction capacity limitation are also used for end bearing capacity limitation [34].

9.1.3 Stability conditions expressions

When uplift resistance and safety factor are evaluated, buoyancy force must be taken into account. Buoyancy uplift force origins in the water pressure difference around a submerged object. From Arquimedes' principle, the buoyancy force is equal to the weight of the displaced fluid []:

$$F_B = \rho_f g V, \tag{34}$$

where ρ_f is the fluid density (kg/m^3), g is the gravity acceleration (m/s^2) and V is the displaced fluid volume.

The whole volume of the structure (both above and bellow the mudline) is considered for the buoyancy calculation (Eq. 34) as the porous of saturated soil are filled with water (and air in the case of partially saturated soils). The downward resistance forces that inhibit the buoyancy forces are the weight of the Engine Reservoir (W_T, Eq. 17) and the weight of the soil filling if applicable (W_S, Eq. 18). The direction of the shear or skin resistance and the bearing resistance developed by the soil depends on the relation between buoyancy and deadweight forces. For net uplift force ($F_B > W_T + W_S$), the shear or skin resistance force acts downwards and there is no end-bearing resistance force. Consequently, the soil provides a uplift resistance capacity of $R_{s,uplift}$ (Eq. 20). Contrarily, when the deadweights overcome the buoyancy and there is a net downwards force ($F_B < W_T + W_S$), the skin and bearing resistances act upwards. In order to evaluate driving or compression situation, it has been defined the soil driving resistance capacity $R_{s,driving}$. Following this argument, the stable equilibrium for vertical loads without considering currents or waves is described through the following inequalities:

$$F_B \leq (W_T + W_S) + Q_f \qquad \text{for} \quad F_B > W_T + W_S \tag{35}$$

$$F_B + Q_f + Q_p \geq (W_T + W_S) \quad \text{for} \quad F_B < W_T + W_S \tag{36}$$

where Eq. 35 refers to the stability against flotation, and Eq. 36 considers the stability against the structure sinking into the soil. It is used the skin friction resistance capacity (Q_f) introduced in Section 9.1.2, which is equivalent to the maximum shear resistance that the soil can provide. From the previous stability inequations, the factors of safety for driving and uplift situations ($SF_{driving}, SF_{uplift}$ correspondingly) are imposed as:

$$\frac{W_T + W_S + Q_f}{F_B} = \overline{SF}_{uplift} \geq SF_{uplift} \tag{37}$$

$$\frac{F_B + Q_f + Q_p}{W_T + W_S} = \overline{SF}_{driving} \geq SF_{driving} \tag{38}$$

where the values of SF_{uplift} and $SF_{driving}$ are to be chosen > 1.

It must be noted that the worst case scenario has been considered for the calculation of the buoyancy force on structures embedded in the seabed. Arquimedes' principle (Eq. 34) has been proven to be suitable for structures embedded on saturated sandy soils. Nevertheless, a decrease on buoyancy force has been observed experimentally for weak-permeable or impervious soils such as cohesive soils due to the interaction between soil and water particle at a micro scale [20]. Therefore, using Arquimedes' principle for both cohesive and cohesiveless soil is a conservative calculation for the case of cohesive soils, that adds a safety factor on the anti-floating calculation.

9.2 Seabed → Structure interactions: Earth Pressures

This section focuses on the earth pressure distribution over depth, and its effect on a buried lateral wall. The expressions have been extracted from literature [14]. Depending on the soil-structure interaction, three types of earth pressures can be considered:

- Active earth pressure: considered when the wall suffers a rotation that causes it to move away from the soil in the earth pressure direction. The minimum rotation for active earth pressure is 2mrad (2mm/m, 2mm of lateral movement per meter of the wall height).

- Passive earth pressure: considered when the walls moves in the soil direction, opposite to the earth pressure direction. The minimal rotation for passive earth pressure is 10mrad or 10mm/m.
- Earth pressure at rest: is the horizontal pressure acting on the rigid structure. It is considered when the structure does not allow deformations big enough to mobilise active or passive earth pressures.

For simplicity, only earth pressure at rest is applied in the structure. It is computed as:

$$\sigma_r = \sigma_z K_0 \tag{39}$$

where σ_r is the earth pressure at rest (N/m^2), σ_z is the vertical normal total stress or overburden stress (N/m^2) and K_0 is the at-rest earth pressure coefficient.
The vertical normal stress (σ_z) is given by:

$$\sigma_z(z) = \int_0^z \gamma_s d\tilde{z} + \gamma_w(z-d) = \sigma'(z) + u(z) \tag{40}$$

where γ_s is the unit weight of the soil (N/m^3), specifically the dry soil unit weight for z above the water level and the submerged or effective soil unit weight (γ' in Table 3,2) for z below the water table. γ_w is the water unit weight (N/m^3), z is the soil depth below the seabed surface (m) and d is the depth of the ground water table bellow the soil surface (negative for water level above the soil surface). Then, the vertical normal stress can be decomposed into the effective stress (σ') caused by the soil, and the water pore or neutral pressure (u).
The at-rest earth pressure coefficient (K_0) is calculated using Terzaghi formula for cohesive soils (Eq. 41) and Jáky expression for cohesionless soils (Eq. 42):

$$K_{0,cohesive} = \frac{\nu}{1-\nu} \tag{41}$$

$$K_{0,cohesionless} = 1 - \sin\phi \tag{42}$$

where ν is the Poisson's ratio and ϕ is the angle of internal friction of the soil. Jáky's coefficient (Eq. 42) has been proven to be also valid for normally consolidated clays []. Then, and due to the high variability of viscosity ν with the soil water content, and the scarcity of viscosity data available for the cohesive soils considered, it has been decided to use Jáky's expression for both cohesive and cohesionless soils.
Additionally, a surface subcharge is considered to account for the water above the seabed. The surface subcharge or vertical surface load causes an increment of the earth pressure ($\Delta\sigma_r$) uniformly distributed along the structure wall as:

$$\Delta\sigma_r = fK_0, \tag{43}$$

where f is the the surface subcharge (N/m^2).

9.3 Fluid → Structure interactions: Hydrostatic and hydrodynamic conditions

The fluid exerts an hydrostatic pressure to the structure, perpendicular to its surface. Additionally, other loads have to be taken into account when the hydrodynamic case of currents is considered. Both situations are described in the subsections below.

At the initial phases of the project, when the Engine Reservoir was treated as located on the sea, literature research was done on finding a general methodology for fitting current data into known velocity profiles expressions and on the selection of the proper wave governing equations given a certain input data. Nevertheless, this research is if less importance for the lake environment conditions, where the currents and waves are relatively small, so the mentioned research has been moved to Appendix B.

9.3.1 Fluid-Structure interaction: Hydrostatic loads

Hydrostatic loads ($\mathbf{F}_{hydrostatic}$) are constituted by pressure forces that the fluid exerts to the structure in no-flow no-wave situation. It is calculated through the surface integral of the hydrostatic pressure (P) that acts normal to the body surface:

$$\mathbf{F}_{hydrostatic} = \iint_S P\mathbf{n}\, dS \tag{44}$$

where $\mathbf{n}$ is the unit vector normal to the surface. Additionally, the value of the hydrostatic pressure only depends on the depth bellow water level (d) and the fluid density (ρ_f), and it is given by:

$$P = \rho_f g d \tag{45}$$

9.3.2 Fluid-Structure interaction: Hydrodynamic or fluid flow loads

The fluid flow exerts a force on the structure surfaces when it passes through it. The hydrodynamic loads can be classified as drag force (parallel to flow direction) and lift force (perpendicular to the flow direction). Furthermore, this forces are the result of two contributors, the pressure force (F_p) and the viscous force (F_v):

$$\mathbf{F}_{hydrodynamic} = \mathbf{F}_p + \mathbf{F}_v. \tag{46}$$

The pressure or pressure-gradient force is generated due to the pressure differences on the body surfaces, and can be computed as detailed in the hydrostatic case (Eq. 44). On the other side, viscous force acts on the opposite direction to the fluid flow and it is generated by the action of the friction force. Both pressure and viscous forces are highly dependant to the flow type. In some cases one of the pressure of viscous forces is clearly dominant, and the other can be neglected.

The approach of pressure and viscous loads discretisation is used on COMSOL simulations in Section 10.3. Additionally, the analytical model of Morison's equation is introduced for simulations verification purposes. The hydrodynamic load model approach uses Morison's equation to calculate the horizontal reaction loads on a submerged cylindrical object. The wave contribution is only valid when the ratio between the waves wavelength and the object diameter is large (> 5). The Morison's equation for a fixed rigid cylinder is [15]:

$$F_h(t) = F_D(t) + F_I(t), \tag{47}$$

where F_h (N/m) is the horizontal hydrodynamic force vector per unit length acting normal to the cylinder axis, F_D (N/m) is the drag force vector per unit length that acts on the cylinder axis and is contained in the plane formed by the member axis and u and F_I (N/m) is the inertia force per unit length that acts normal to the cylinder axis and is contained in the plane formed by the cylinder axis and $\dot{u}$.

The drag force per unit length is given by:

$$F_D(t) = \frac{1}{2} C_D \rho D u(t)|u(t)|, \tag{48}$$

where $u(t)$ (m/s) are the fluid velocity that is horizontal and normal to the cylinder axis, ρ (kg/m^3) is the fluid density and D is the cylinder diameter and C_D is the drag hydrodynamic coefficient. The horizontal velocity $u(t)$ can also be decomposed as:

$$u(t) = u_w(t) + u_c, \tag{49}$$

where $u_w(t)$ is caused by the waves and u_c is associated to the current velocity profile and it is assumed constant in time. As for the drag hydrodynamic coefficient, it depends on the shape of the object that opposes to the flow and the flow velocity (and specifically the flow Reynolds number). There is no exact expression that relates C_D with the object shape and flow velocity, but there are plots available that relate C_D with the Reynolds number Re. The coefficient C_D for the design case of circular cylindrical object is obtained by substituting Reynolds number (Re, Eq. 50) in Fig.

?? for a specific flow velocity and cylinder diameter. The Reynolds number for a circular cylinder is found as [26]:

$$Re = \frac{\rho u D}{\mu}, \tag{50}$$

where rho is the fluid density (kg/m^3), u is the flow speed (m/s^2), D is the cylinder diameter (m) and μ is the fluid dynamic viscosity ((N·s)/m^2 or kg/(m·s)).
The inertia force per unit length can be calculated as:

$$F_I(t) = C_M \rho \frac{\pi D^2}{4} \dot{u}(t), \tag{51}$$

where C_M is the inertia hydrodinamic coefficient and $\dot{u}(t)$ (m/s^2) is the fluid acceleration that is horizontal and normal to the cylinder axis. For the case of no waves and assumed constant current velocity profile, the inertia force is null as the fluid has no horizontal acceleration.

The transverse or vertical force component is characterised by the lift force caused by the largest flow velocities on the top of the structure. When the flow encounters the structure, it must pass over the structure or laterally. Then, higher flow velocities on the top of the structure cause lower pressure, which will induce a vertical lift force perpendicular to the flow velocity (upwards). The vertical lift force per unit length is given by:

$$F_v(t) = F_L(t) = \frac{1}{2} C_L \rho D u^2(t), \tag{52}$$

where C_L is the lift hydrodynamic coefficient.

9.4 Rigid Reservoirs and Flexible Bladders Connection Loads

The connections loads describe the forces and momentum's exerted by the Flexible Bladders and the Rigid Reservoir. For the case of the Rigid Reservoir, it is assumed that d_{buried} is large enough so that the soil weight and frictions prevent the reservoir from lifting for the critical case of the empty reservoir (when the buoyancy force is maximum). Then, the connection between the Engine Reservoir and the Rigid Reservoir just involves fluid flow, and the loads from the Rigid Reservoir to the Engine Reservoir are negligible ($F_{RR-ER} \approx 0N, M_{RR-ER} \approx 0Nm$).

The loads caused by the Flexible Bladder must be analysed in more detail, as it is not buried into the seabed. The stakeholder Ocean Grazer is working on the Flexible Bladder subjection on the seabed, which will be done through a system of cables supported by embedded anchors or the (buried) Rigid Reservoir. It is worth highlighting that the Flexible Bladder net vertical force is relatively small, as the buoyancy force (F_b) is expected to be very similar to the gravity force (F_g). As the flexible hermetic reservoir adapts its volume to the volume of contained water, it should not contain air at any moment of the Ocean Battery working cycle. Then, the buoyancy net force ($F_b - F_g$) is only caused by the small difference of density between the exterior lake water and the interior fluid, and the relatively thin exterior layer of the flexible bladder. For the case of the fluid within the flexible bladder, stakeholder Ocean Grazer have chosen fresh water. As the fluid inside the Flexible Bladder is the same as the exterior lake fresh water, there is no net buoyancy force. Consequently, the bladder net buoyancy force is caused only by the bladder material as:

$$F_{net} = V_{bladder} g (\rho_w - \rho_{bladder}), \tag{53}$$

where $V_{bladder}$ is the thickness volume of the bladder membrane, g is the gravity acceleration and ρ_w and $\rho_{bladder}$ are the densities of the water and the bladder material correspondingly. For the Flexible Bladder material, previous Ocean Grazer projects worked with Ethylene Propylene Diene Monomer rubber (EPDM) [21] of density $\rho = 20kg/m^3$[3]. No information have been found regarding the relation between EPDM material and the Flexible Bladder capacity. Moreover, commercially available pillow tanks have a maximum capacity of $2000m^3$ approximately, which is smaller than the minimum capacity required of $3000m^3$ (Fig. 7(a)). Nevertheless, for the sake of getting an approximate idea of the order of magnitude of the net buoyancy force on the flexible

bladder, it is assumed that the Flexible Bladder resembles a pillow tank of capacity $3000 \sim 6000m^3$ (Fig. 7 and $P = 1MW$). Linyi Solpac Co. claims to be able to produce a pillow tank of $100m^3$ of thickness $d = 1.2mm$[8]. Roughly scaling the thickness to $d = 36mm$ for a pillow tank of capacity $3000m^3$, and choosing a square base pillow tank of dimensions [L x W x H] = 45m x 45m x 1.5m (capacity of 3037m^3), the bladder volume can be approximately calculated as:

$$V_{bladder} = (L + 2d)(W + 2d)(H + 2d) - LWD. \tag{54}$$

Substituting the pillow tank parameters into Eq. 54 and Eq. 53, it is obtained $V_{bladder} = 77.88m^3$ and $F_{net} = 7.49 \cdot 10^5 N \approx 750kN$. Although it might seem a significantly large force, the Rigid Reservoir withstands a buoyancy force caused by $O(10^3)m^3$ of air ($3000m^3$ in the case of P=1MW and $d_{buried} = 50m$), while the Flexible Bladder net buoyancy is only caused by $77.88m^3$ of bladder material, which has a density relatively close to air density. Therefore, it is considered that the Rigid Reservoir has very large axis bearing capacity and can make the function of retaining the Flexible Bladder through a net of ropes (or similar) that are subjected by the Rigid Reservoir. As a conclusion, the connection loads or interaction between the Flexible Bladders and the Engine Reservoir is also neglected.

10 Model setup

10.1 Model I. Stability conditions on structure uplift and driving and soil load carrying capacity (Matlab)

Model I analyses the structure stability of Design I regarding the phenomena of uplift and driving and with respect to the structure embedded depth. Therefore, the uplift and driving safety factors are compared with the existing vertical forces using the inequations from Section 9.1. To do so, the geotechnical load carrying capacity, the sliding friction resistance and the end bearing resistance are calculated as in Section 9.1.2. The structure geometry is taken from Tab. 5, and its location with respect to the mudline is taken as a variable in order to study at a embedded depth influence over uplift and driving phenomena ($d_{buried} \in (0, 50)m$). Additionally, a parametric study on the satisfaction of the safety factors is performed for 7 types of soil (Tab. 2, 3).

Design I uses reinforced cement concrete for all the structure elements (Section 8.2). Model I weight calculations use concrete density $\rho_c = 2.400kg/m^3$ and approximated reinforcement ratios per structural element from Tab. 4. For the sake of simplicity and due to uncertainty on Design I, it is only considered the building elements of Bases, Slabs and Retaining Walls.

The results from Model I have been analysed previous to the construction of the next models. An adequate embedded depth d_{buried} is chosen from the study of Model I results, and it is taken as input data by the next models. Additionally, all the next models are done with Design II, which has more optimised dimensions than Design I.

10.2 Model II. Fluid → Porous Seabed Interaction (Comsol)

The model studies the effect of soil saturation on the soil. Soil saturation is the phenomena of a fluid filling the soil porous or space between soil particles, and it appears when the soil is located below the water level or water table. Then, the fluid fills the soil porous driven by gravity forces (free flow) or due to applied load or pressure (forced flow). A completely saturated soil, or a soil of 100% saturation, describes a porous soil where all the porous are filled with water. In the studied case of the Engine Reservoir environment, the porous soil is located on the lake bottom. The seabed surface is in direct contact with the fluid, and the fluid exerts a large and evenly distributed hydrostatic pressure on the seabed. Therefore, it is expected that the soil is completely saturated. Nevertheless, the different layers of soil might produce alterations into the fluid flow and pore pressure. The extreme case is when the soil contains impermeable layers; the fluid cannot penetrate them, and therefore the pore pressure drops to zero.

Model II works with the limit case of completely saturated soil. It considers only one layer of soil (constant characteristics with depth) and it is characterised as porous and permeable. Additionally, the approximation of completely horizontal soil is used, which makes possible to use a 2D space where the second coordinate y accounts for depth. The setting for the model geometry, material, physics and multi-physics are described below:

- Geometry: 2d space with fluid domain (D2) and porous soil domain (D1). The domains dimensions account for the water level of 35m and the maximum buried depth of 50m (Fig. 12).
- Materials: water (fluid) for domain D2 and seabed soil (porous media) for domain D1. The seabed soil materials considered are Kaolin Clay and Silica Sand, the properties relevant for the studies are detailed in Table 7.
- Physics: Free and Porous Media Flow with Free and Porous Media Flow interface (D1 and D2) and Solid Mechanics (D1). The physics boundary conditions described in Tab. 8 using the boundary numbering detailed in Fig. 12.
- Multiphysics: Free and Porous Media Flow and Solid Mechanics interfaces are coupled. The boundaries where multiphysics is applied are detailed in Tab. 8 using the boundary numbering detailed in Fig. 12.

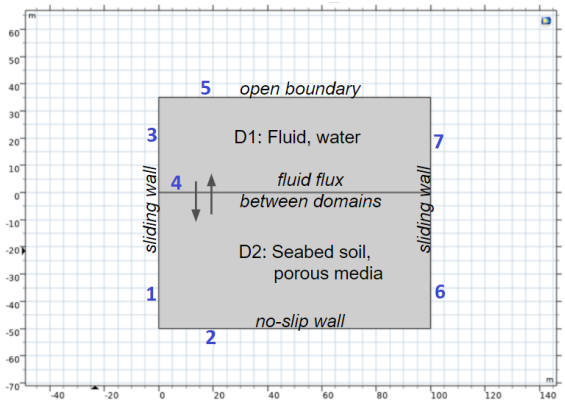

Figure 12: Geometry and free and porous media flow boundary conditions of model I. Boundary numbering in blue.

Parameter Name	Symbol	Kaolin Clay	Silica Sand	Unit
Effective soil weight	γ'	5993	6500	[N/m^3]
Young Modulus	E	10 - 200	10 - 50	[MPa]
Poisson's ratio	ν	0.2 - 0.4	0.15 - 0.35	-
Porosity	n_s	33-60	20-35	%
Permeability	k_s	10^{-9} - 10^{-6}	10^{-5} - 10^{-3}	[cm/s]

Table 7: Soil parameters used on Model II [4]

It should be noted that COMSOL Multiphysics includes several interfaces to study the fluid flow within a porous media, each one based in different equations and assumptions. Within the physics of Free and Porous Media Flow, the following interfaces can be used: Darcy's Law, Fracture Flow, Richard's Equation, Brinkman Equations, Free and Porous Media Flow, Phase Transport in Porous Media and Multiphase Flow in Porous Media [10]. Fig. 14 shows the adequate governing equations (used by the before mentioned interfaces) of each soil region. From the figure, it is concluded that the adequate governing equation are Navier-Stokes equations for the fluid domain and Brinkman Equations for the porous soil domain. Then, the interface Free and Porous Media Flow is suitable for the model, as it solves Navier-Stokes equations in the fluid and Brinkman equations in the soil.

10.3 Model III. Fluid → Structure Interaction (Comsol)

Model III aims to study the loads and moments on the structure caused by the fluid hydrostatic loads (pressure) and the hydrodynamic loads derided from the current. Furthermore, the impor-

Boundary	Free and Porous Media Flow (D1,D2)	Solid Mechanics (D1)
1	Wall, slip / Symmetry	Roller / Symmetry
2	Wall, no-slip	Fixed Constant
3	Wall, slip / Symmetry	-
4	Multiphysics, fully coupled	Multiphysics, fully coupled
5	Open boundary, No Normal Stress	-
6	Wall, slip / Symmetry	Roller / Symmetry
7	Wall, slip / Symmetry	-

Table 8: Boundary conditions of the physics in Model II, using the boundary nomenclature detailed in Fig. 12

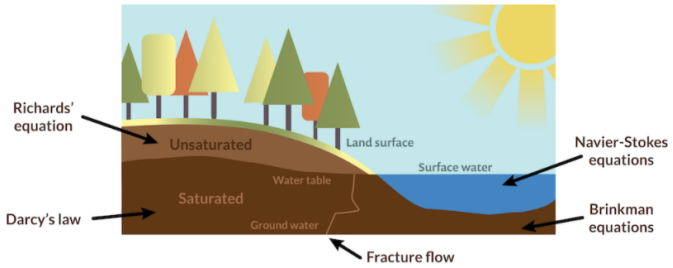

Figure 13: Schematic view of the cross-section of a river bank. Specified the governing equations of the fluid flow for each soil region [].

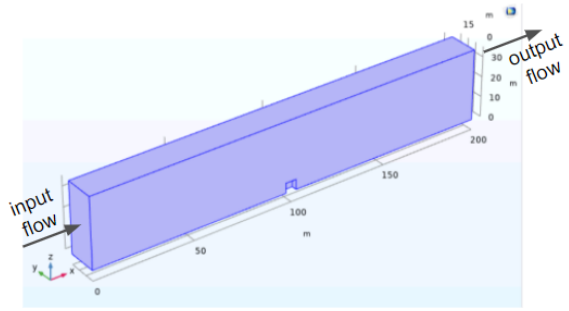

Figure 14: Geometry and boundary conditions of Model III.

tance of current modelling for the purpose of the Engine Reservoir analysis will evaluated through the comparison between hydrostatic pressure derived forces and current derived forces.

As stated in Section 9.3, the interaction between fluid and structure is not fully coupled but simplified as one-way interaction (from the fluid to the structure). Then, only the effects of the fluid to the structure are considered (such as hydrostatic pressure, viscous forces) and the effects of the structure to the fluid (such as fluid field change due to structure displacement) are neglected. As a result, it is enough to model only the fluid domain in order to evaluate the effect of the fluid to the structure. Accordingly, the model consists on one 3d fluid domain, and the structure is added in the form of domain difference. The Engine Reservoir above the mudline consists on the upper part of the shaft, with 5m of height and a square planar area of 4m x 4m; the fluid domain difference is relatively small compared with the size of the fluid domain. It is considered the limit case when the current is perpendicular to one of the structure faces, as it is the case when the interaction loads are expected to be more significant. Then, it can be used the simplification of only modelling half of the domain on y-axis due to symmetry on the xz-plane (using coordinate system from Fig. 14).

The model geometry is a single fluid domain of dimensions 200m x 15m x 35 m, with a difference of dimensions 5.4m x 2.7m x 5m and centred on (100,0,0)m that represents (half) of the structure above the mudline. Fig. 14 shows the orthographic projection of the geometry. As for the physics utilised, the fluid domain is modelled as Turbulent Flow with k and ϵ as turbulent parameters. The boundary conditions are no sliding wall for domain bottom (fluid boundary with the seabed), sliding wall for the upper (water surface) and lateral boundaries, and inlet and output for opposing boundaries perpendicular to x-axis (Fig. 14). The inlet velocity field is chosen perpendicular to the boundary surface, and it is used a normal state velocity profile. In order to get the velocity profile, data from Appendix A is taken for the currents normal state, and it is fitted in Section **??** as predominantly tidal current profile.

Some comments should be done on the subject of fluid forces calculation method. From the solution to the microscopic momentum balance or Navier-Stokes equation, it is found the body surface loads

caused by the fluid flow ($\underline{F}$) []:

$$\underline{F} = \iint_s (\hat{n} \cdot \underline{\underline{\Pi}})|_{surface} dS, \tag{55}$$

where $\underline{\underline{\Pi}}$ the total stress 2nd order tensor, $\hat{n}$ is the unit normal vector to infinitessimal surface dS and S is the macroscopic body surface that interacts with the fluid. In accordance with the hydrostatic loads description in Section 9.3.2, the total stress tensor have the contribution of a viscous term and a pressure term:

$$\underline{\underline{\Pi}} = \underline{\underline{\hat{\tau}}} - p\underline{\underline{I}}, \tag{56}$$

where $\underline{\underline{\hat{\tau}}}$ is the viscous stress tensor, p is the fluid pressure and $\underline{\underline{I}}$ is the identity tensor. Finally, for Newtonian fluids (such as water) the viscous stress tensor depends on fluid velocity as:

$$\underline{\underline{\tilde{\tau}}} = \mu(\nabla \underline{v} + (\nabla \underline{v})^T) \tag{57}$$

In Comsol implementation, total force is calculated through the surface integration of $\underline{T}$, the total stress vector on a surface at a particular location with unit normal vector:

$$\underline{T} = (\hat{n} \cdot \underline{\underline{\Pi}})|_{surface} = \begin{bmatrix} \text{spf.T\_stressx} \\ \text{spf.T\_stressy} \\ \text{spf.T\_stressz} \end{bmatrix} \tag{58}$$

Analogously, the viscous force is calculated through the surface integration of $\underline{K}$, the viscous stress vector on a surface at a particular location with unit normal vector $\hat{n}$:

$$\underline{K} = (\hat{n} \cdot \underline{\underline{\tilde{\tau}}})|_{surface} = \begin{bmatrix} \text{spf.K\_stressx} \\ \text{spf.K\_stressy} \\ \text{spf.K\_stressz} \end{bmatrix} \tag{59}$$

10.4 Model IV. Porous Seabed → Structure Interactions (Matlab)

Model IV studies the stress loads caused by the porous soil to the structure surfaces. Specifically, it is calculated the Lateral Earth Pressure at-rest on the structure lateral surfaces and the pore water pressure over soil depth. The model is governed by the soil equations presented on Section 9.2. For the sake of briefly, only two types of soil have been tested by the model: Kaolin Clay and Silica Sand (Tab. 2,3). This two soils have been selected because they present significantly different properties; the results comparison will provide information about which are the significant properties on soil pressures calculation and the nature of its influence. By assuming completely saturated soil, the vertical normal stress is calculated as in Eq. 40. For the water pore pressure calculation, it has been considered the soil top level at 35m below the water level ($z_{mudline} = 35m$). For accounting for the extra pressure due to the 35m of water above the soil, it is equivalent to compute pore pressure taking $d = -35m$ in Eq. 40 than taking $d = 0m$ and adding an uniformly distributed load with a surface subcharge of $f = \gamma_w g z_{mudline}$ in Eq. 43.

10.5 Model V: Integrated Model (Comsol)

Model V is called Integrated Model because it accounts for the interactions between Fluid, Soil and Structure, studied in previous models. Each medium or domain is driven by a set of governing equations, that can be implemented in COMSOL through Physics and Physics Interfaces. The interactions between mediums are introduced by the determination of boundary conditions and by Multiphysics interface. The governing equations of each domain or sub-model are described in the following subsections 10.5.1, 10.5.2 and 10.5.3.

The three numerical sub-models described below are to be integrated in COMSOL using Arbitrary Lagrangian-Eulerian (ALE) mesh (moving mesh), boundary conditions described in Section 10.5.5, seabed parameters from Table 9 and the following Physics:

- (Fluid domain) 'Laminar Flow' Physics with incompressible fluid for Navier-Stokes sub-model

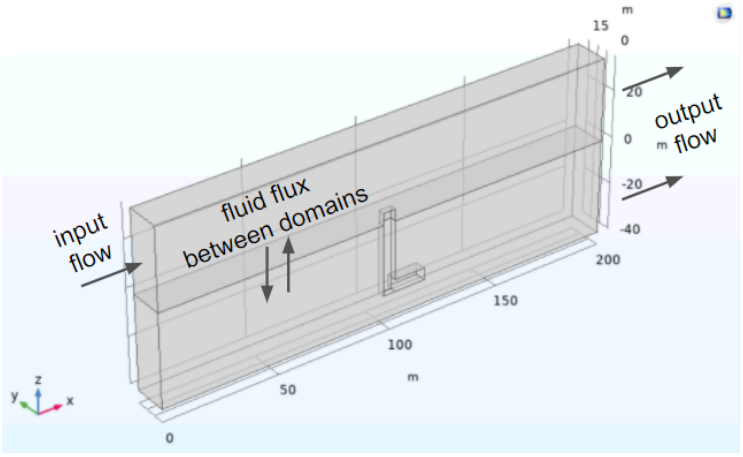

Figure 15: Geometry and boundary conditions of Model V

- (Seabed domain) 'Porous Media and Subsurface Flow' Physics with 'Darcy's Law' or 'Free and Porous Media Flow' interfaces.
- (Structure domain) 'Solid Mechanics' Physics
- (Interaction between Physics) 'Poro-elasticity' Multiphysics

Unfortunately, the COMSOL Multiphysics licence provided by University of Groningen do not include the licence for 'Subsurface Flow Module', required for the seabed Physics and the 'Poro-elasticity' Multiphysics. Consequently, it has been taken an alternative approach for seabed modelling, which consists on introducing the seabed sub-model governing equations (Section 10.5.2) in the form of Partial Differential Equations (Section 10.5.4) using 'Coefficient Form PDE' Physics. Nevertheless, no results are presented for Model V because the Stationary Study did not converge. At this point, Model V has been simplified as Model VI in order to obtain study convergence and valuable results.

Variables	Symbol	Value	Unit
Porosity	n_s or ϵ	0.4	-
Permeability	k_s	10^{-3}	m/s
Shear modulus	G	$5 \cdot 10^8$	N/m^2
Poisson's ratio	μ_s	0.33	-
Saturation	S	0.98	-
True modulus of water elasticity	K_w	$2 \cdot 10^9$	N/m^2

Table 9: Model VI porous seabed parameters

10.5.1 Governing equations of the fluid sub-model

Fluid velocity field and pressure distribution is described by Navier-Stokes equations (NS). In some particular where turbulence phenomena plays an important role, might be adequate to use the time-averaged Reynolds-Averaged-Navier-Stokes equations (RANS). Through the imposition of momentum balance in terms of stress, it is obtaned the generalised equations of the fluid flow in terms of velocity gradients and fluid pressure:

$$\rho \frac{\partial \vec{u}}{\partial t} - \nabla \cdot [\eta(\nabla \vec{u} + (\nabla \vec{u})^T)] + \rho(\vec{u} \cdot \nabla)\vec{u} + \nabla p_f = \vec{F}, \tag{60}$$

$$\nabla \cdot \vec{u} = 0, \tag{61}$$

where ρ is the fluid density, η is the fluid dynamic viscosity, $\vec{u}$ is the fluid velocity field, p_f is the pressure and $\vec{F}$ is a volumetric force, the gravity in the case studied.

10.5.2 Governing equations of the seabed sub-model

Seabed sub-model bases on Biot's poro-elastic theory [] , which treats the seabed as a compressible porous medium with a flow of a compressible pore fluid. The governing equation for mass conservation is given by:

$$\nabla \cdot (K \nabla p_s) - \gamma_w n_s \beta_s \frac{\partial p_s}{\partial t} = \gamma_w \frac{\partial \varepsilon_s}{\partial t} \tag{62}$$

where ∇ is the divergence operator ($\nabla = \frac{\partial}{\partial x} + \frac{\partial}{\partial y} + \frac{\partial}{\partial z}$), p_s is the pore pressure (Pa), γ_w is the unit weight of the pore water, n_s is the soil porosity, β_s is the compressibility of the seabed pore water pressure and ε_s is the volumetric strain. Assuming the seabed to be homogeneous and isotropic, that is to say, with the same permeability k_s in all directions, Eq. 62 can be rewritten as:

$$\nabla^2 p_s - \frac{\gamma_w n_s \beta_s}{k_s} \frac{\partial p_s}{\partial t} = \frac{\gamma_w}{k_s} \frac{\partial \varepsilon_s}{\partial t}, \tag{63}$$

where Δ is the Laplace operator ($\Delta = \frac{\partial^2}{\partial x^2} + \frac{\partial^2}{\partial y^2} + \frac{\partial^2}{\partial z^2}$). The compressibility of the pore fluid can be denoted as:

$$\beta = \frac{1}{K_w} + \frac{1 - S}{P_w}, \tag{64}$$

where K_w is the true modulus of water elasticity ($\mathrm{N/m^2}$), S is the soil degree of saturation and P_{w0} is the absolute static water pressure. The volumetric strain is defined as:

$$\varepsilon_s = \nabla \cdot \vec{u}_s = \frac{\partial u_s}{\partial x} + \frac{\partial v_s}{\partial y} + \frac{\partial w_s}{\partial z}, \tag{65}$$

where $\vec{u}_s = (u_s, v_s, w_s)$ is the soil displacement vector and its decomposition in xyz-direction.

The relationship of stress-strain (between pore pressure and soil displacement) for the force equilibrium is given by:

$$G \nabla^2 \vec{u}_s + \frac{G}{1 - 2\mu_s} \nabla \varepsilon_s = \nabla p_s, \tag{66}$$

where G is the soil shear modulus and μ_s is the soil Poisson's ratio. Eq. 66 can be decomposed as:

$$G \frac{\partial^2 u_s}{\partial x^2} + \frac{G}{1 - 2\mu_s} \frac{\partial \varepsilon_s}{\partial x} = \frac{\partial p_s}{\partial x} \tag{67}$$

$$G \frac{\partial^2 v_s}{\partial y^2} + \frac{G}{1 - 2\mu_s} \frac{\partial \varepsilon_s}{\partial y} = \frac{\partial p_s}{\partial y} \tag{68}$$

$$G \frac{\partial^2 w_s}{\partial z^2} + \frac{G}{1 - 2\mu_s} \frac{\partial \varepsilon_s}{\partial z} = \frac{\partial p_s}{\partial z} \tag{69}$$

and the shear modulus G is related to the soil Young's modulus (E) and the Poisson's ratio (μ_s) as:

$$G = \frac{E}{2(1 + \mu_s)} \tag{70}$$

The equilibrium equations in the three coordinate directions that impose force equilibrium are given by []:

$$\frac{\partial \sigma'_x}{\partial x} + \frac{\partial \tau_{xy}}{\partial y} + \frac{\partial \tau_{xz}}{\partial z} = \frac{\partial p_s}{\partial x} \tag{71}$$

$$\frac{\partial \tau_{yx}}{\partial x} + \frac{\partial \sigma'_y}{\partial y} + \frac{\partial \tau_{yz}}{\partial z} = \frac{\partial p_s}{\partial y} \tag{72}$$

$$\frac{\partial \tau_{zx}}{\partial x} + \frac{\partial \tau zy}{\partial y} + \frac{\partial \sigma'_z}{\partial z} = \frac{\partial p_s}{\partial z} \tag{73}$$

where σ'_x, σ'_y and σ'_z are the effective normal stresses in xyz-direction, τ_{xy}, τ_{xz}, τ_{yx}, τ_{yz}, τ_{zx} and τ_{zy} are the effective shear stresses and p_s is the pore pressure. Then, the expressions of effective normal and shear stresses can be obtained by substituting Eq. 71-73) in Eq. 67-69:

$$\sigma'_x = 2G\Big[\frac{\partial u_s}{\partial x} + \frac{\mu_s}{1-2\mu_s}\varepsilon\Big] \tag{74}$$

$$\sigma'_y = 2G\Big[\frac{\partial v_s}{\partial y} + \frac{\mu_s}{1-2\mu_s}\varepsilon\Big] \tag{75}$$

$$\sigma'_z = 2G\Big[\frac{\partial w_s}{\partial z} + \frac{\mu_s}{1-2\mu_s}\varepsilon\Big] \tag{76}$$

$$\tau_{xy} = \tau_{yx} = G\Big[\frac{\partial u_s}{\partial y} + \frac{\partial v_s}{\partial x}\Big] \tag{77}$$

$$\tau_{xz} = \tau_{zx} = G\Big[\frac{\partial u_s}{\partial z} + \frac{\partial w_s}{\partial x}\Big] \tag{78}$$

$$\tau_{yz} = \tau_{zy} = G\Big[\frac{\partial y_s}{\partial z} + \frac{\partial w_s}{\partial y}\Big] \tag{79}$$

It is worth mentioning that the governing equations regarding the force balance use the Terzaghi's principle of effective stress. It states that the soil total stress (σ_{ij}) can be decomposed into the soil effective stress (σ'_{ij}) and the soil pore pressure (p_s) as:

$$\sigma_{ij} = \sigma'_{ij} + \delta_{ij} p_s, \tag{80}$$

where δ_{ij} refers to the Kronecker delta.

10.5.3 Governing equations of the structure sub-model

The structure sub-model bases on small-displacements assumption. It is used the following relationship between strain and displacement components:

$$\varepsilon_x = \frac{\partial u}{\partial x}, \quad \varepsilon_{xy} = \varepsilon_{yz} = \frac{1}{2}\big(\frac{\partial u}{\partial y} + \frac{\partial v}{\partial x}\big), \tag{81}$$

$$\varepsilon_y = \frac{\partial v}{\partial y}, \quad \varepsilon_{yz} = \varepsilon_{zy} = \frac{1}{2}\big(\frac{\partial v}{\partial z} + \frac{\partial w}{\partial y}\big), \tag{82}$$

$$\varepsilon_z = \frac{\partial w}{\partial z}, \quad \varepsilon_{xz} = \varepsilon_{zx} = \frac{1}{2}\big(\frac{\partial u}{\partial z} + \frac{\partial w}{\partial x}\big), \tag{83}$$

where the displacement field is $\vec{u} = (u, v, w)$ in the system coordinates (x, y, z) and the strain tensor ε is given by:

$$\varepsilon = \begin{bmatrix} \varepsilon_x & \varepsilon_{xy} & \varepsilon_{xz} \\ \varepsilon_{yx} & \varepsilon_y & \varepsilon_{yz} \\ \varepsilon_{zx} & \varepsilon_{zy} & \varepsilon_z \end{bmatrix}. \tag{84}$$

Analogously, the structure stress tensor is defined as:

$$\sigma = \begin{bmatrix} \sigma_x & \tau_{xy} & \tau_{xz} \\ \tau_{yx} & \sigma_y & \tau_{yz} \\ \tau_{zx} & \tau_{zy} & \sigma_z \end{bmatrix}. \tag{85}$$

Using the strain and stress tensors described above, the structure behaviour is modelled using the assumption of linear elastic behaviour between stress and strain:

$$\sigma = D_m \varepsilon, \tag{86}$$

where D_m is the elasticity matrix, and the weak formulation of the equilibrium conditions in terms of stress:

$$-\nabla \cdot \sigma = \vec{F}, \tag{87}$$

where $\vec{F}$ accounts for volume or body forces.

10.5.4 PDE Coefficients for seabed sub-model

Governing equations of the seabed sub-model (Section **??**) are implemented in Comsol Multiphysics through Physics module 'Coefficient Form PDE'. With pore pressure (p_s) as dependent variable, the general expression of the PDE (Partial Differential Equation) is:

$$e_a \frac{\partial^2 p_s}{\partial t^2} + d_a \frac{\partial p_s}{\partial t} + \nabla \cdot (-c\nabla p_s - \alpha p_s + \gamma) + \beta \nabla p_s + a p_s = f, \tag{88}$$

where c is the diffusion coefficient (m/s), a is the absorption coefficient (1/m·s), f is the source term (kg/m^2·s^3), e_a is the mass coefficient (s/m), d_a is the damping coefficient (1/m), α is the conservative flux convection coefficient (1/s), β is the convection coefficient (1/s) and γ is the conservative flux source (W/m^3). The coefficient values are chosen to so that the general PDE (Eq. 88) represents the governing equation for mass conservation from Biot's poro-elastic theory and for isotropic seabed (Eq. 63). Then, all coefficients are chosen null except for:

$$c = -k_s \tag{89}$$

$$d_a = -\gamma_w n_s \beta_s \tag{90}$$

$$f = \gamma_w \frac{\partial \varepsilon_s}{\partial t} \tag{91}$$

10.5.5 Boundary Conditions

Define boundary conditions, relate with sub-models

- Structure - Seabed: no-slip boundary
  It is assumed that the structure has the same displacement and velocity as the seabed, there is no relative displacement between seabed and structure (Eq. 92). Additionally, as the structure is considered rigid and inelastic, there is a null normal gradient of pore water pressure (Eq. 93). The total stress equilibrium at the boundary is given by Eq. 94.

  $$u_s = u_{st} \tag{92}$$

  $$\frac{\partial p_s}{\partial n} = 0 \tag{93}$$

  $$\sigma_{st} = \sigma'_s, \quad \tau_{st} = \tau_s \tag{94}$$

  where subscript 's' accounts for soil domain, and 'st' for structure domain.

- Structure - Fluid Boundary: no-slip boundary
  The structure normal stress is determined by the fluid (Eq. 95), while the moment shear stress is neglected (Eq. 96).

  $$\sigma_{st} = -p_f \tag{95}$$

  $$\tau_{st} = 0, \tag{96}$$

  where P_f is the normal stress that the fluid exerts normally to the structure.

- Fluid - Seabed (seabed surface): no-slip boundary
  It is assumed that the soil has null vertical effective stress and null shear stress (Eq. 97) and that the pore water pressure of the seabed is given by the fluid pressure on the boundary (Eq. 98).

  $$\sigma'_s = 0, \quad \tau_s = 0 \tag{97}$$

  $$p_s = p_f \tag{98}$$

- Seabed underlying bottom: it is assumed that the seabed boundaries with an impenetrable material; there are no displacements, no pore water pressure gradient and no normal vertical flow.

  $$u_s = v_s = w_s = 0 \tag{99}$$

  $$\frac{\partial p_s}{\partial n} = 0 \tag{100}$$

- Seabed side boundaries: it is assumed zero displacement for side boundaries sufficiently far from the embedded structure.
- Fluid inlet: (piston) wave-maker generates the waves. Constant current velocity profile over time.
- Fluid outlet: sponge layer to reduce the wave reflection.
- Fluid surface: free boundary
  Free boundary implies zero pressure applied (except from a reference pressure of p_{ref} = 1atm).

10.6 Model VI - Integrated model II (Comsol)

The attempt to simultaneously model and simulate all the mediums (fluid, seabed and structure) and its interactions through Model V has failed. Therefore, Model VI has been developed as a simplification of Model V. It models only the structure domain, but it applies as boundary loads the known one-way interactions between mediums studied in previous models.

Model VI works in 3D space and models the structure geometry using Design II parameters and embedded depth $d_{buried} = 30m$ below seabed surface. As for the materials, the initial approach was to directly model the reinforced concrete, combining concrete and steel domains and taking into account the interactions between them through Solid Mechanics boundary conditions. Nevertheless, this procedure has been found not adequate for COMSOL Multiphysics due to convergence errors and high uncertainty of the geometry of the reinforcement. Consequently, the structure has been modelled using pure concrete material. The result analysis will provide information whether reinforcement is necessary for the given structure design.

The Physics used is Solid Mechanics, and no Multiphysics interfaces are required. The boundary conditions on the structure-fluid boundary ($z > 0m$) are extracted from the results of Model III (Sections 11.3, whose analysis conclude that he fluid loads to the structure are mainly due to hydrostatic pressure, and that the effects of fluid flow can be neglected. Accordingly, the boundary condition for structure surfaces for $z > 0m$, being $z = 0m$ the height of the seabed surface, is given in terms of pressure as:

$$P(z) = \gamma_w g(d_{seabed} - z), \tag{101}$$

where $d_{seabed} = 35m$ is the depth of the seabed surface with respect to the water level. The boundary conditions on the structure-seabed boundary ($z < 0m$) are taken from Model IV results. Accordingly, the so-called lateral earth pressures at-rest are applied on the structures surfaces below the seabed surface ($z < 0m$). Additionally, for the horizontal structure surface buried on the seabed (ceiling of the Machines Hall) no lateral earth pressure has been applied but the combination of pore pressure and filling soil weight. It is worth mentioning that the soil weight is calculated using the effective or submerged soil weight, referred as γ' along the report. All boundary conditions are represented graphically in Fig. 16.

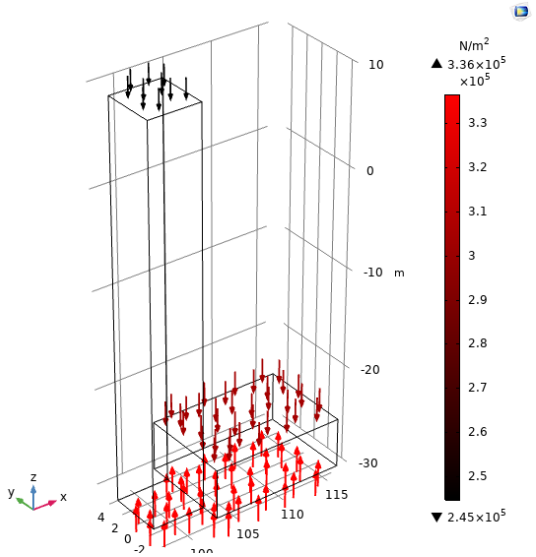

(a) Vertical earth pressures for $z < 0m$ and vertical hydrostatic pressures for $z > 0m$.

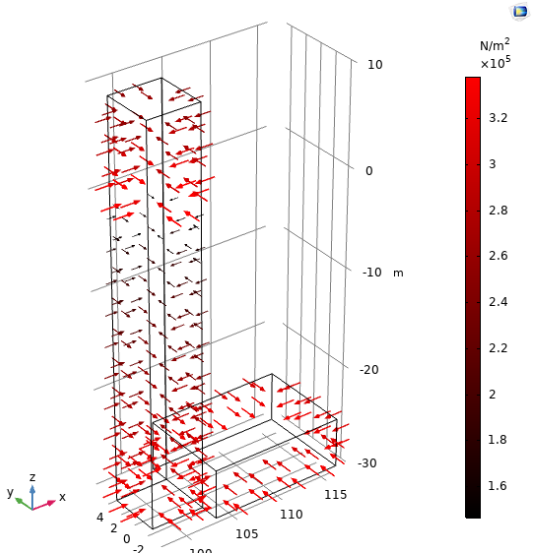

(b) Lateral earth pressures at-rest for $z < 0m$ and horizontal hydrostatic pressures for $z > 0m$.

Figure 16: Surface boundary loads as pressures applied on the structure external surface due to the one-way interactions of the fluid and seabed to the structure.

10.7 Model VII - Reinforced structure (Cypecad)

Finally, Model VII is developed with the goal of providing a complete mechanical study that takes into account the surface loads exerted by the environment, the structure self-weight and hydropower components loads and the steel reinforcement contribution. It uses $d_{buried} = 30m$ and $d_{seabed} = 35m$ for loads computation and Silica Sand (Table 2) for soil thrust calculation. Nevertheless, the model allows to change these design and environment parameters easily.

The Engine Reservoir is structured in 5 levels or floors, as shown in Figure 18. The height, description and structural loads of the floors are detailed in Table 10. The table differentiates two types of structural loads:

- Dead loads: also known as permanent or static loads, they are the relatively constant loads over time.
- Life loads: also known as imposed loads, they refer to dynamic loads or temporary loads. They are the variable forces over the normal operation cycle of the structure.

As observable in the table, Cypecad works with superficial and evenly distributed loads in t/m^2, where t accounts for tones. The superficial dead loads for the Engine Reservoir ceiling P5 ($30t/m^2$) and for the Machines Hall ceiling P3 ($46t/m^2$) are directly obtained using the expressions for hydrostatic pressure and the (effective) soil weight above P3. The life load applied on the Exchange Room Floor accounts for replacement operations of hydro-power machines. Assuming a moving mechanism that works as an elevator along the Engine Reservoir Shaft, the elevator temporary load has been chosen as the weight of 5 persons and 1 hydropower machine. Using the approximate values of 80kg/person and 600kg/machine (extracted from reversible pump-turbine weight calculation in Section 7.2, the total temporary weight is $1000kg = 1t$. In order to account for the self-weight of the elevator structure, an additional $1t$ has been added to the calculation. Then, the surface life load is $2t$ evenly distributed on a 4m x 4m surface, which results in a surface load of $0.13t/m^2$. Finally, P2 dead load of $1t/m^2$ is obtained from the weight of the hydro-power machinery and water conveyance system. Using the approximation that the weight is evenly distributed along the floor, and that all the penstock weight (and filling water) is supported by the floor. Assuming

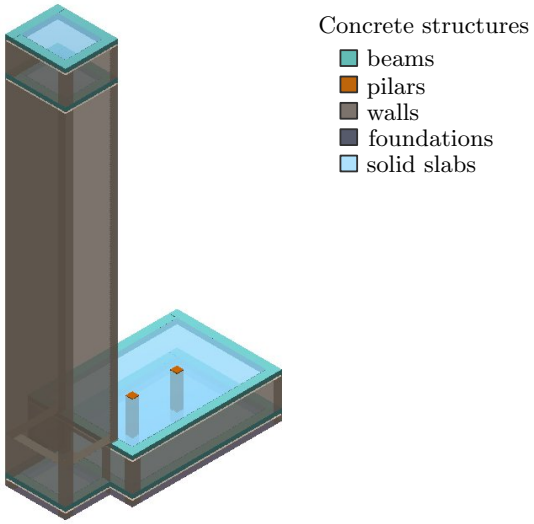

Figure 17: Cypecad 3D representation of the Engine Reservoir model.

Floor Name	Height [m]	Level [m]	Length x Depth [m x m]	Life Loads (L) [t/m^2]	Dead Loads (D) [t/m^2]
P5	3	5	[4 x 4]	0	30
P4	28	2	[4 x 4]	0.13	0
P3	3	-26	[12 x 8] + [4 x 4]	0	46*
P2	1	-29	[12 x 8] + [4 x 4]	0	1*
P1	-	-30	[12 x 8] + [4 x 4]	0	0

Table 10: CYPECAD floors description. *Surface loads only applied on [12 x 8] floor region.

maximum penstock diameter ($D_{p,max} \approx 1m$ from Section 7.2), penstock completely full of fluid, 4 reversible pump-turbines

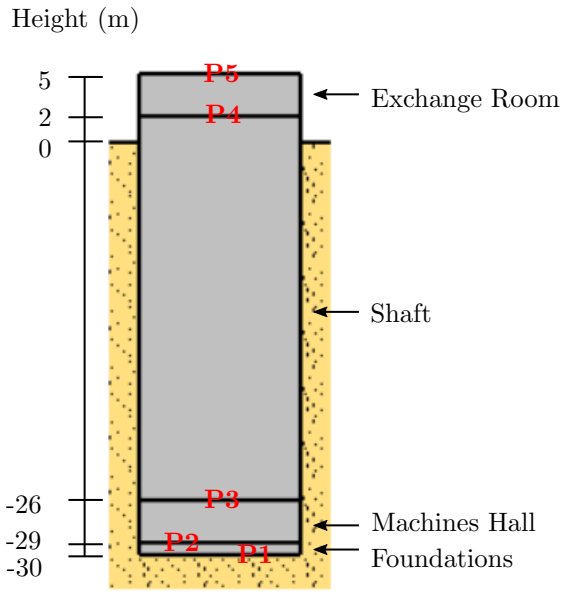

Figure 18: Visualisation of Cypecad floors. Height defined with the origin in the seabed surface.

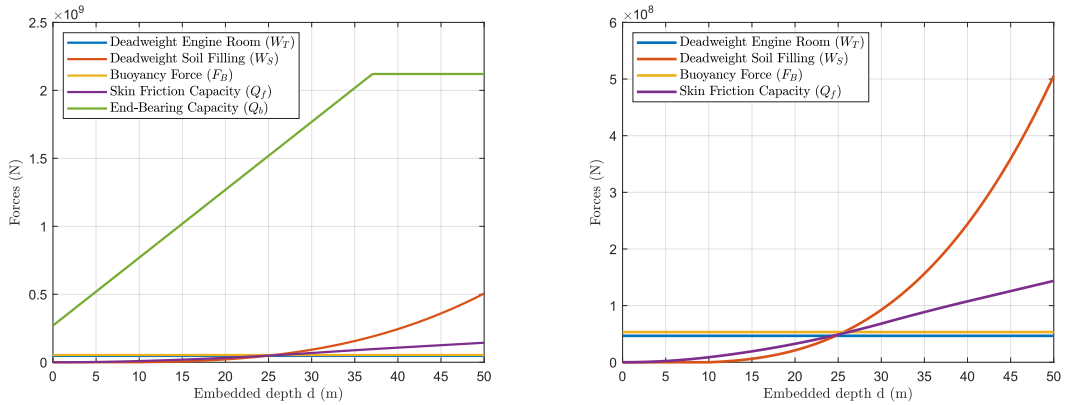

(a) (b)

Figure 19: Parametric study on ER embedded depth of static ER deadweights, buoyancy and soil capacities. Soil considered: Silica Sand, cohesionless.

11 Simulation Results

11.1 Results Model I

The results for (cohesionless) Silica Sand are presented in detailed in Fig. 19, 20. It is easy to observe the bearing capacity Q_p is significantly bigger than the rest of vertical forces and capacities, therefore the safecty factor against buoyancy is satisfied without problems ($\overline{SF}_{driving} > SF_{driving}$ for all embedded depths $d \in (0, 50)m$). Converselly, the safety factor against driving or sinking is only satisfied for embedded depths bigger than a critical value, in this case $d_{critical} \approx 20m$ (where $\overline{SF}_{uplift} > SF_{uplift}$).

From the results presented for Silica Sand, it is decided to compare the critical requirement (satisfaction of SF_{uplift}) for multiple cohesive and cohesionless soils. The results are compared in Fig. 21. It is observed that Design I must be embedded at least $15m$ to satisfy the safety factor against uplift. Additionally, cohesionless soils show better resistance against uplift, that is to say, the minimal embedded depths that satisfies uplift safety factor is smaller for cohesionless soils. Additionally, it is also observed that Nkossa Clay and Kaolin Clay perform the worst in the uplift safety factor satisfaction and they are also the less dense cohesionless soils.

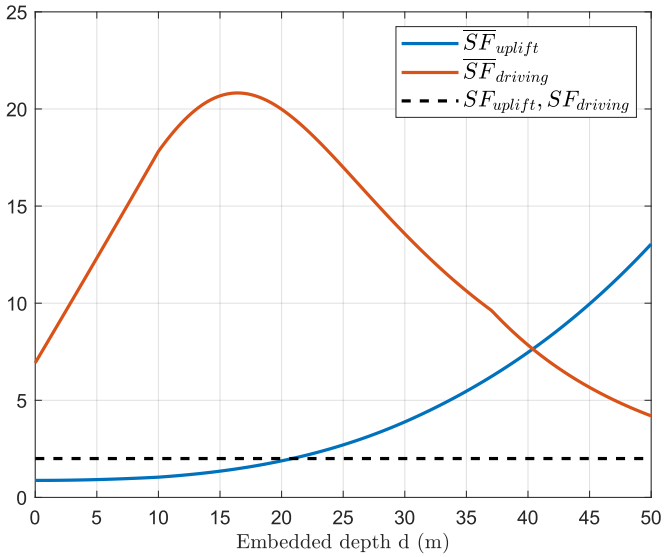

Figure 20: Parametric study on ER embedded depth of stability safety factors against uplift and driving. Soil considered: Silica Sand, cohesionless.

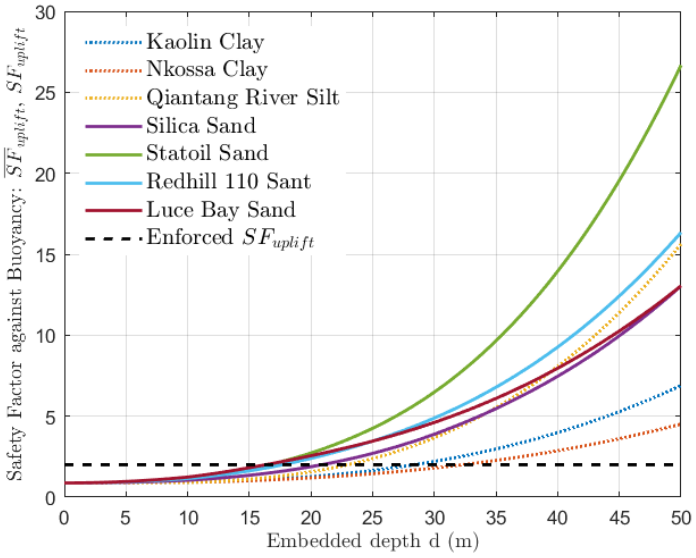

Figure 21: Parametric study on ER embedded depth of stability safety factor against uplift (SF_{uplift}) for multiple cohesive (continuous curves) and cohesionless (dotted curves) soils.

11.2 Results Model II

Model II results on Figure 22 show the expected behaviour of the effective vertical stresses and pore pressure. The pore pressure increases linearly with depth, as expected from the expressions on Section 9.2. Additionally, Figure 22 show the linear increase of the effective earth stresses from the mudline, also as expected from Section 9.2 expressions. It is worth mentioning that the relatively small pressures of silica sand are caused by its relative smaller density with respect to Kaolin Clay. It is also observed a large difference between the soil effective stresses (continuous lines) and the lateral earth stresses at-rest (dashed lines).

Additionally, soil displacement along y-coordinate is studied for the soils ranges of Young Modulus (E). It is clear to see from Fig. 23 that the soil is suffering a compression, and furthermore this soil displacement is inversely proportional to Young Modulus. The displacement order of magnitude if of O(-1).

11.3 Results Model III

11.3.1 Fluid-Structure Interaction: Hydrostatic loads

11.3.2 Fluid-Structure Interaction: Hydrodynamic loads

The hydrodynamic pressure and viscous forces introduced in Section 9.3.2 are calculated in Comsol as detailed in Section 10.3. The values of the total load and its contributions (pressure and viscous forces) are calculated for the whole body (integration over all the surface) and for certain structure surfaces in order to get a better understanding of the results.
The total hydrodynamic force (F) for all structure surfaces and its contributions, the pressure force (F_p) and the viscous force (F_v), are:

$$F = \begin{bmatrix} 289.30 \\ 0 \\ -8.5632e6 \end{bmatrix} N, \quad F_p = \begin{bmatrix} 288.27 \\ 0 \\ -8.5632e6 \end{bmatrix} N, \quad F_v = \begin{bmatrix} 1.0269 \\ 0 \\ 0.13572 \end{bmatrix} N \tag{102}$$

where the y-component of the loads is null due to the structure symmetry in y axis and the consideration of perfectly perpendicular flow in x-direction.

The surface loads results for each face are presented individually in Table 11. Small calculations have been made to extrapolate the half-space Comsol simulation to the results for each face, as the Comsol result only provided with the loads recieved in half of Face A,B and C and all Face D. Therefore, for Face A,B and C and for all the loads (F_p, F_v and F), the x,z-components have been multiplied per 2, and the y-components have been set to 0 per symmetry. This calculations can only be made for fluid flow in x-direction and perpendicular to Face A, as in the case of the simulation.

The Comsol simulation gives as a result the fluid pressure in the hydrodynamic case in all fluid domain (p). This result is compared with the theoretical hydrostatic pressure ($p*$), computed analytically as in Eq. 45. Both pressures are compared through their difference ($p - p*$), as in Fig. 27 for a certain vertical line. Moreover, the integrated values of the (analytical) hydrostatic pressure in the structure surfaces are compared with the integrated values of the pressure difference in the same structure surfaces. The obtained integrated values differ by 3 orders of magnitude:

$$\text{Half Face A:} \quad p* = 4.2964e6\,Pa, \quad p - p* = -1.3734e3\,Pa \tag{103}$$

$$\text{Half Face C:} \quad p* = 4.2832e6\,Pa, \quad p - p* = -1.5607e3\,Pa \tag{104}$$

$$\text{Face D:} \quad p* = 8.5928e6\,Pa, \quad p - p* = -3.0992e3\,Pa \tag{105}$$

$$\tag{106}$$

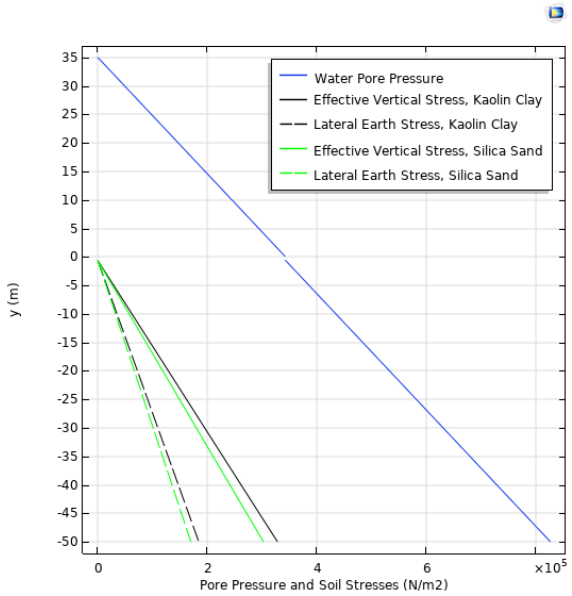

Figure 22: Effective vertical stress and lateral earth stress at-rest for Kaolin Clay (black) and Silica Sand (green). Pore water pressure (blue) for both types of soil.

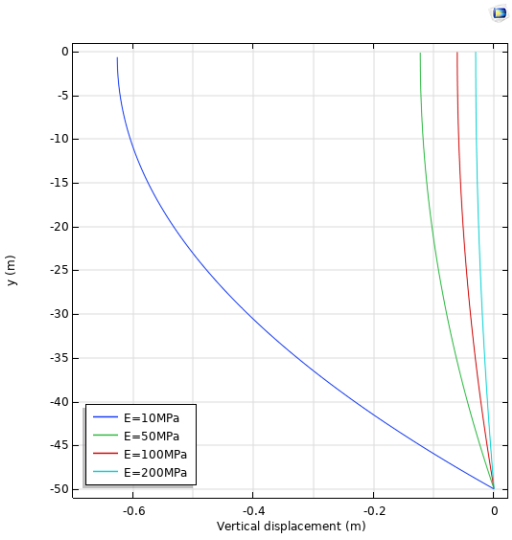

(a) Seabed soil: Kaolin Clay

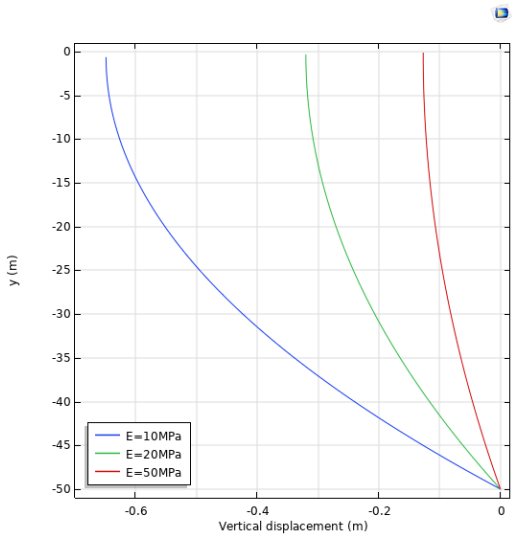

(b) Seabed soil: Silica Sand

Figure 23: Soil displacement along soil depth for different values of Young Modulus for soil type (a) Kaolin Clay and (b) Silica Sand.

	Pressure Force (N)	Viscous Force (N)	Total Force (N)
Face A	$\begin{bmatrix} 8.590e6 \\ 0 \\ -2.785\text{e}{-11} \end{bmatrix}$	$\begin{bmatrix} 0.295 \\ 0 \\ -0.096 \end{bmatrix}$	$\begin{bmatrix} 8.590e6 \\ 0 \\ -0.096 \end{bmatrix}$
Face B	$\begin{bmatrix} -8.590e6 \\ 0 \\ 1.330\text{e}{-8} \end{bmatrix}$	$\begin{bmatrix} -1.388\text{e}{-4} \\ 0 \\ 0.121 \end{bmatrix}$	$\begin{bmatrix} -8.590\text{e}{-6} \\ 0 \\ 0.121 \end{bmatrix}$
Face C	$\begin{bmatrix} 4.204\text{e}{-15} \\ 0 \\ -8.563e6 \end{bmatrix}$	$\begin{bmatrix} 0.514 \\ 0 \\ 0.107 \end{bmatrix}$	$\begin{bmatrix} 0.514 \\ 0 \\ -8.563e6 \end{bmatrix}$
Face D	$\begin{bmatrix} 4.204e-15 \\ -8.590e6 \\ -1.132\text{e}{-9} \end{bmatrix}$	$\begin{bmatrix} 0.109 \\ 0.105 \\ 0.002 \end{bmatrix}$	$\begin{bmatrix} 0.109 \\ -8.590e6 \\ 0.002 \end{bmatrix}$

Table 11: Caption

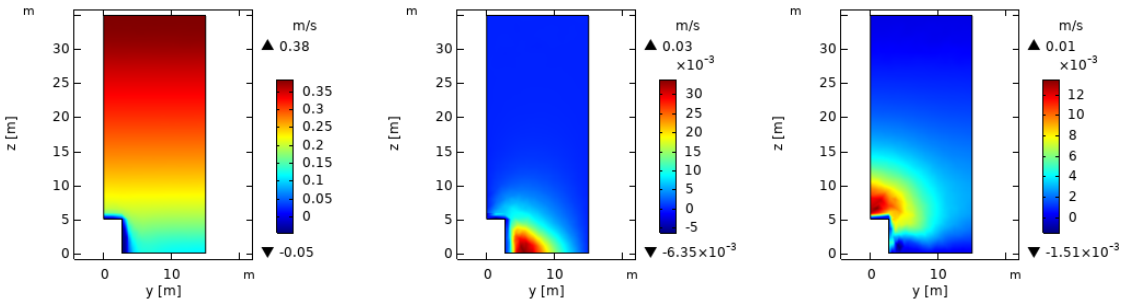

(a) Velocity field yz-plane, x component (m/s)

(b) Velocity fiels yz-plane, y component (m/s)

(c) Velocity field yz-plane, z component (m/s)

Figure 24: Plane representation of the fluid velocity field. Decomposition of the fluid velocity field in x,y,z-components in yz-plane in x=100m (structure centre in x-direction).

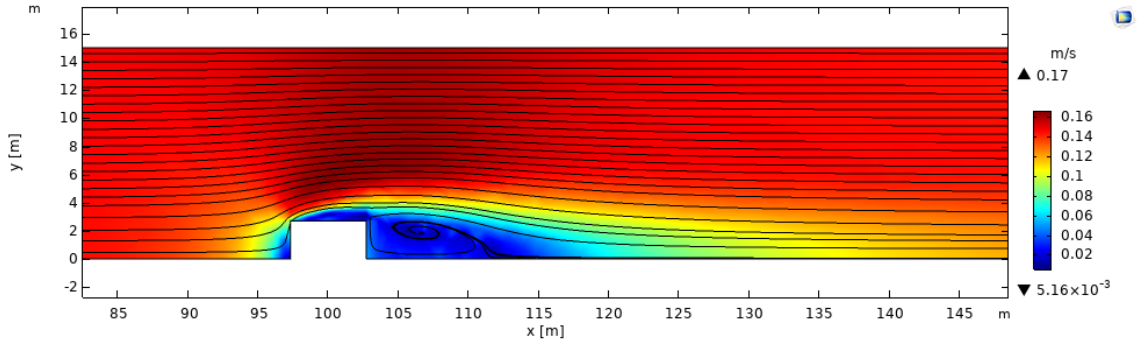

(a) Velocity magnitude xy-plane, z=3.33m, zoomed in

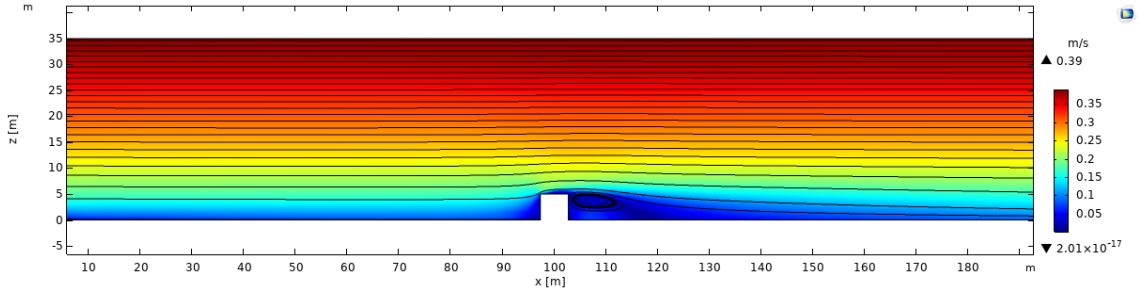

(b) Velocity magnitude xz-plane, y=0m

Figure 25: Plane representation of the fluid velocity on significant xy and xz-planes. Velocity magnitude (m/s) surface and velocity field streamlines.

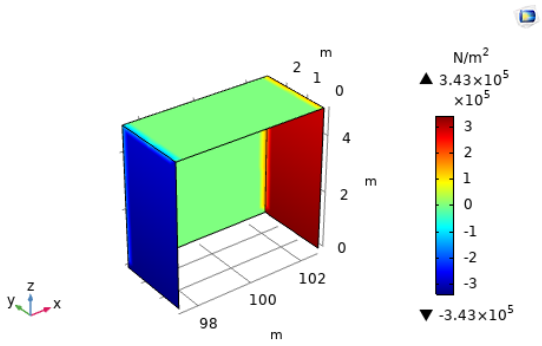

(a) Total stress, x component (N/m^2)

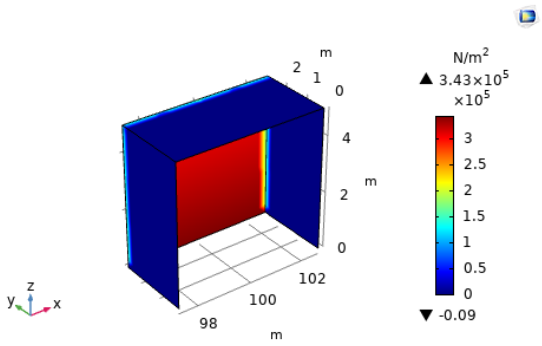

(b) Total stress, y component (N/m^2)

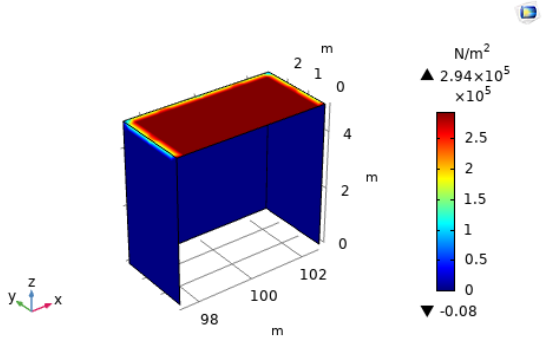

(c) Total stress, z component (N/m^2)

Figure 26: Total stress distribution on the structure surface on interaction with the fluid. Decomposition of the total stress in x,y,z-direction.

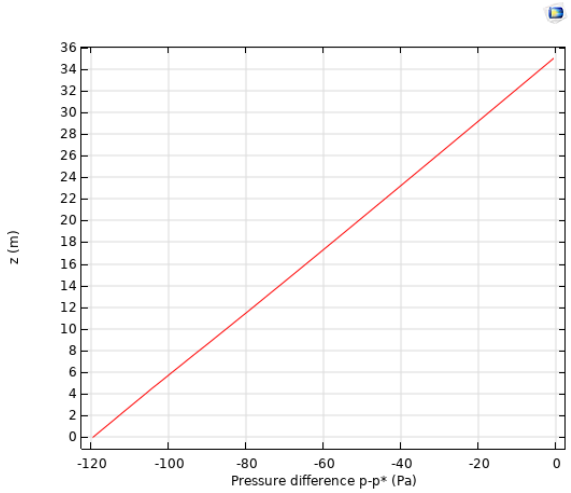

Figure 27: Pressure difference between the simulated hydrodynamic pressure (p) and the hydrostatic pressure (p*) calculated analytically (Eq. 45). The hydrodynamic pressure profile ($p(z)$) is taken from the simulation for $x = 97.3m$ and $y = 0.01$ and $z \in (0, 35)$, which corresponds to a vertical line along the fluid domain and that is contained in the surface of the Face A.

11.4 Results Model IV

The results of Model IV are an analytical implementation of the expressions presented in Section 9.1.2. By comparing the results for Kaolin Clay in Fig. 28 with the Model II COMSOL results also for Kaolin Clay (Fig. 22, black dashed line) it is obtained the same result for lateral earth stress. That is to say, Models II and IV are verified.

11.5 Results Model VI

The effect of the Fluid and Seabed interactions is shown in the model results. Firstly, Fig. 29 show the 3 principal stresses distribution and direction along the structure surface. The 1st principal stress plot (a) shows a stress concentration on the Machine Hall ceiling pointing downwards (negative values of the stress) and shear stress at the shaft. As for the 2nd principal stress, it accounts for shear stresses on the Machine Hall ceiling, and downwards stresses on the shaft and on the Machine Hall ceiling. Finaly, plot (c) accounts for the shear stress of the surfaces studies.

Additionally, Von Mises stress is plotted in Fig. 30. It is show again that the larges stresses are located on the Machine Hall ceiling and lateral surfaces. The central linear surface of the shaft also have significant stress. Finally, Von Mises stress accumulated in the interior edges of the machines Hall.

The displacement result on Fig. 23 show the consequences of the stress concentration on the Machine Hall ceiling observed before: there is a maximum downwards displacement of 3.61mm of the centre of the structure. Additionally, a small tilt of approximately 2.5mm is observed on the top of the shaft.

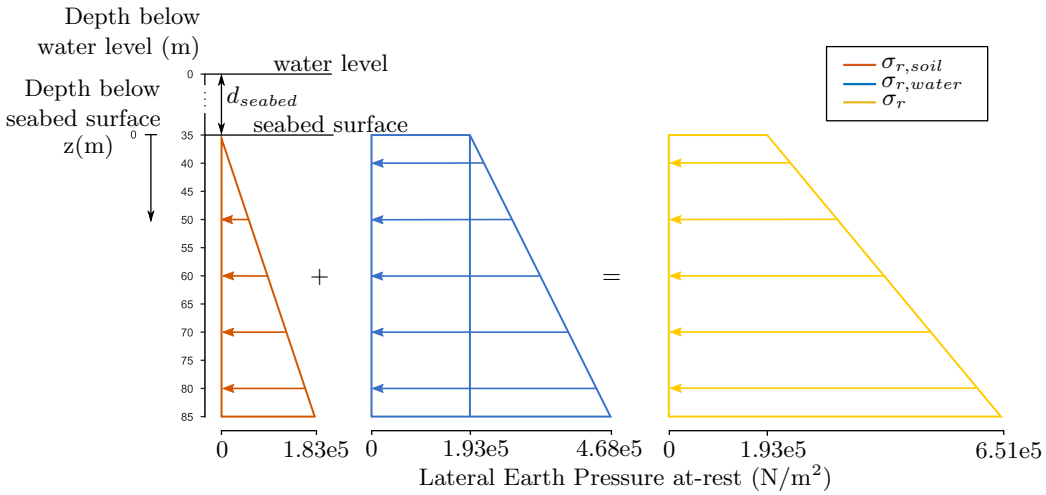

Figure 28: Lateral earth pressure at-rest as a function of depth below the seabed surface ($\sigma_r(z)$). Used $d_{seabed} = 35m$ and soil parameters of Kaolin Clay (Table 2).

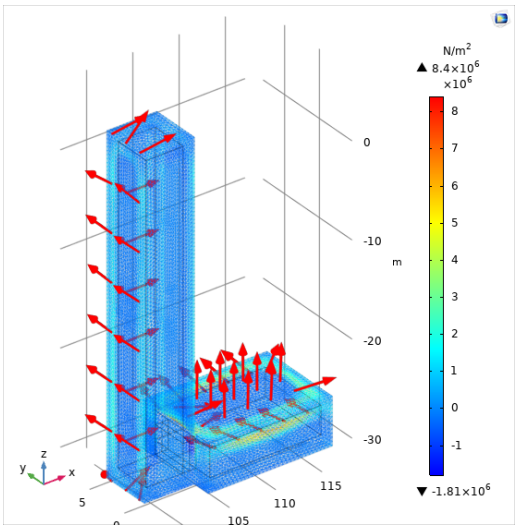

(a) First Principal Stress (N/m^2)

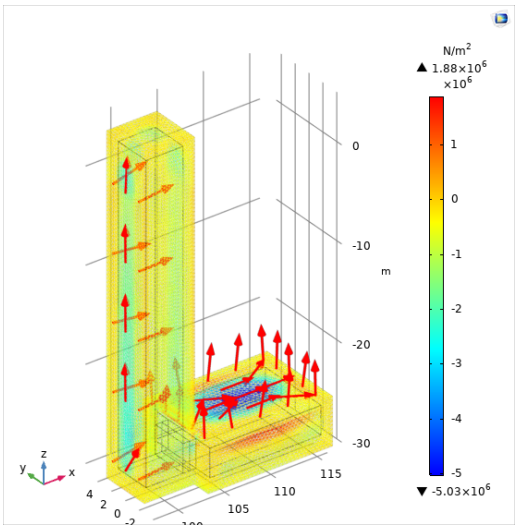

(b) Second Principal Stress (N/m^2)

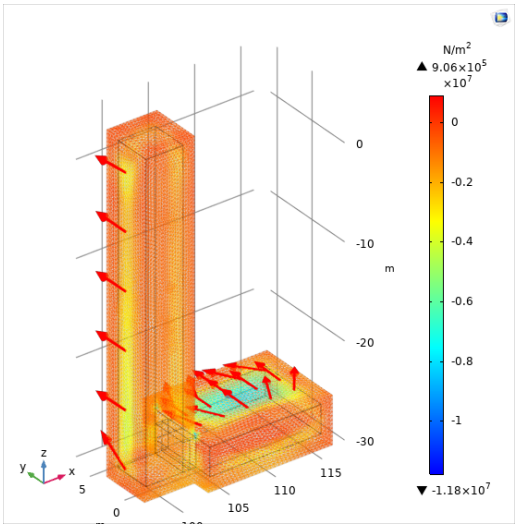

(c) Third Principal Stress (N/m^2)

Figure 29: First, second and third principal stresses on the structure external surface due to one-way interaction of fluid and seabed to the Engine Reservoir. Stress magnitudes as surface plot, stress directions as arrows.

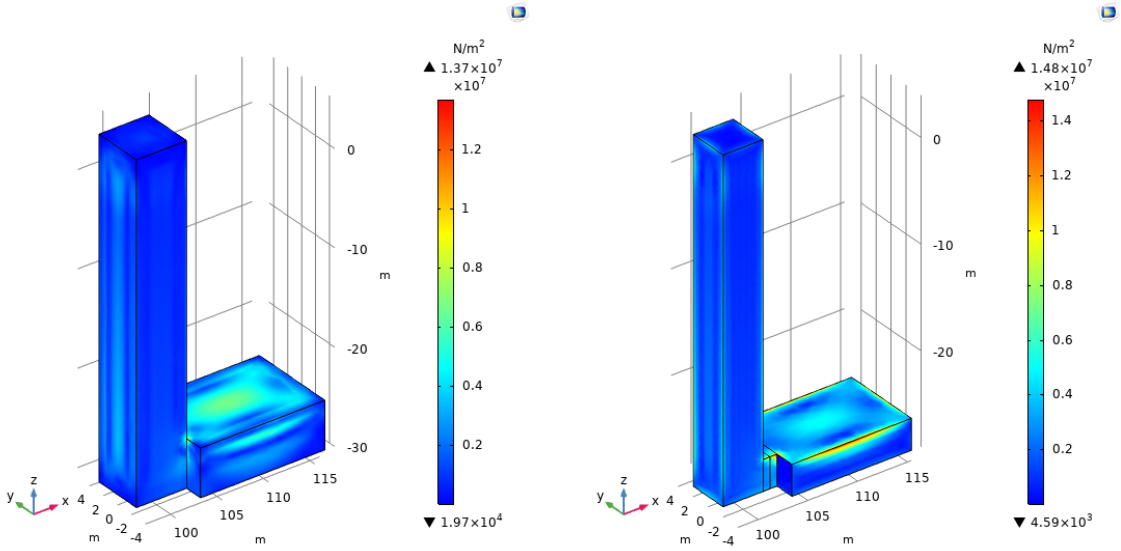

(a) Walls External Surface

(b) Walls Internal Surface

Figure 30: Von Mises stress (N/m^2) for the external (a) and internal (b) wall surfaces of the Engine Reservoir structure.

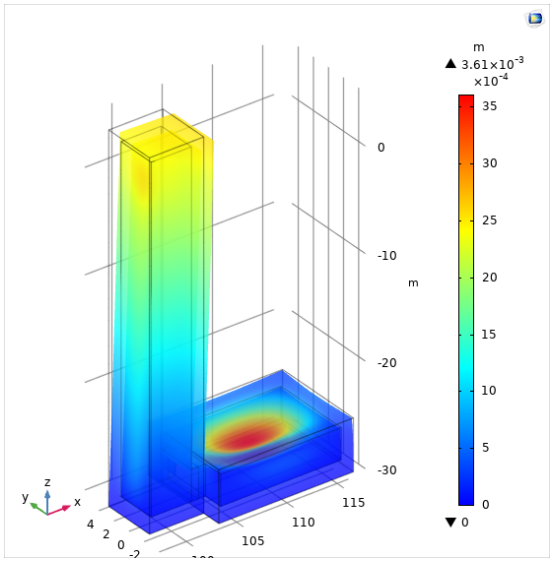

Figure 31: Total displacement magnitude (m) and scaled deformation of the Engine Reservoir external wall surface using pure concrete walls.

11.6 Results Model VII

Model VII generates a enormous quantity of results, as it details the reinforcement for every structural component of the structure. It has only been added the more relevant results for the results analysis, but the rest of results are accessible through CYPECAD model.

Total displacement is shown in Fig. 32. It is again observed a maximum displacement on the middle of the Machine Hall of 2.97mm. It differs from the Model VI maximum displacement for 0.66mm. Nevertheless, the displacement on the shaft top is of order of magnitude O(-1) mm. Figure 33(a) shows the z-displacement of the Machine Hall; its maximum value at the centre is -2.97mm and corresponds with the maximum total displacement found previously. Therefore, it is clear to see that displacement z clearly predominates over x and y displacements. The momentum distributions on subplots (b) and (c) show clearly the effect of the ceiling bending downward from the centre. Figure 34 shows the desired phenomena of the columns absorbing the shear stress, both the x-direction and y-direction shear stresses.

Additionally, subplots from Fig 35 represent the (averaged) ratio of needed reinforcement. As observable, the recommended reinforcement distribution for the inferior and the superior reinforcement (with respect to slab centre) greatly differs, as well as for the inferior x and y-direction reinforcement.

Finally, the results for the reinforcement calculations are presented in Fig. 36. The cross at the middle of the floor means there is a base reinforcement, and the additional lines (as in (b)) specify the additional reinforcement that has been considered suitable for the loads applied. P2 and P5 slabs have only base reinforcement, but P3, which refers to the Machine Hall ceiling, has a very significant ratio of reinforcement, with a base grid of steel bars. A more clear data is obtained when the quantities of material used are evaluated and presented in Tab. 12 and Fig. 36(a,b). A very large amount of material is required for the project construction: 59357 kg of steel bars and 671 m^3 of concrete. Furthermore, Fig36(a) shows P4 is the floor with highest material domain for both concrete and steel, as it contains most of the Engine Reservoir Shaft. It is also worth mentioning the high requirement of steel in P3, which refers to the dense reinforcement of the Machine Hall ceiling.

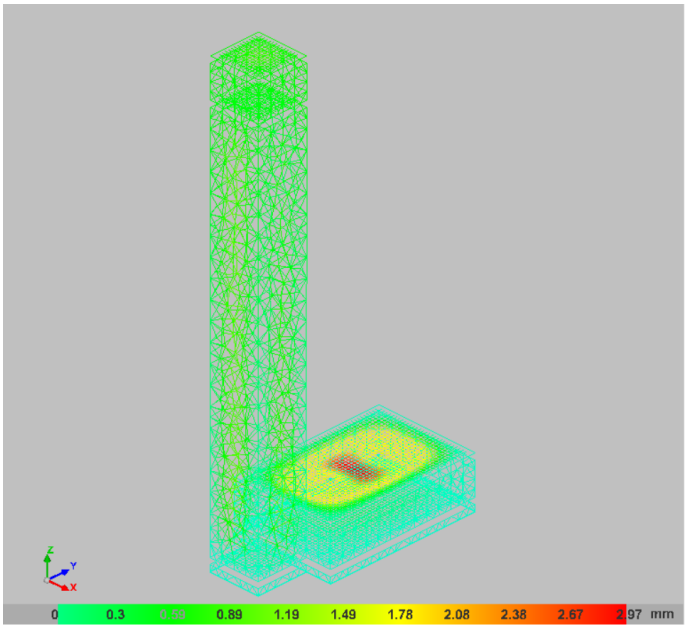

Figure 32: 3D representation of the deformation suffered on the Engine Reservoir walls, slabs and pillars.

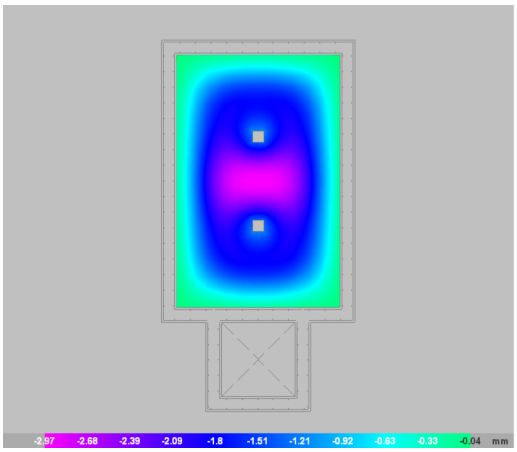

(a) Displacement, z-direction (mm)

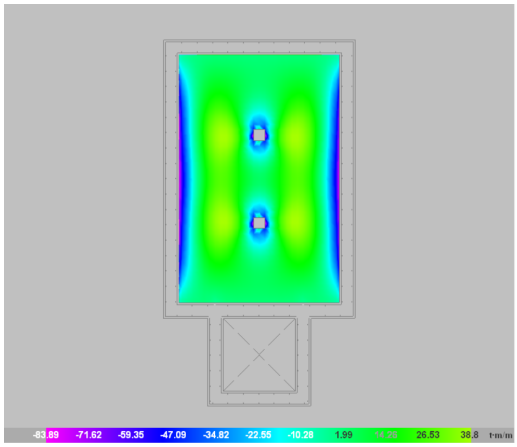

(b) Moment, x-direction (t·m/m)

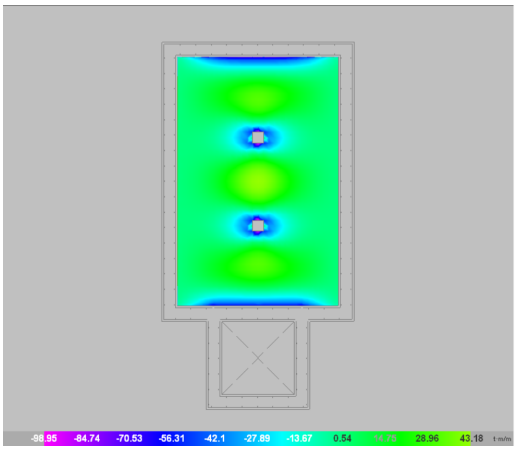

(c) Moment, y-direction (t·m/m)

Figure 33: Displacement in z-direction and moments in x,y-direction on the upper concrete slab of the Machines Hall.

Total project - Total surface: 327.78 m²

Element	Surface (m²)	Volume (m³)	Bars (kg)
Slabs	196.65	98.32	6511
*Rein. base slabs			9799
Beams	130.13		
Lateral shuttering	64.90		
Walls	1632.05	571.22	41674
Pillars (Sup. Shuttering)	12.00	1.50	1373
Total	2035.73	671.04	59357
Index (per m²)	6.211	2.047	181.09

Table 12: Project summary in terms of concrete surface (m^2), concrete volume (m^3) and reinforcement steel bars mass (kg).

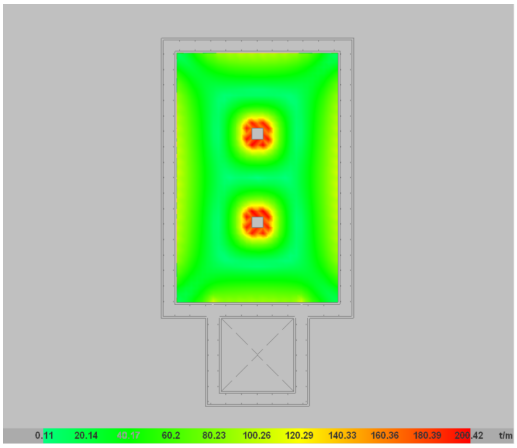

(a) Total shear stress (t/m)

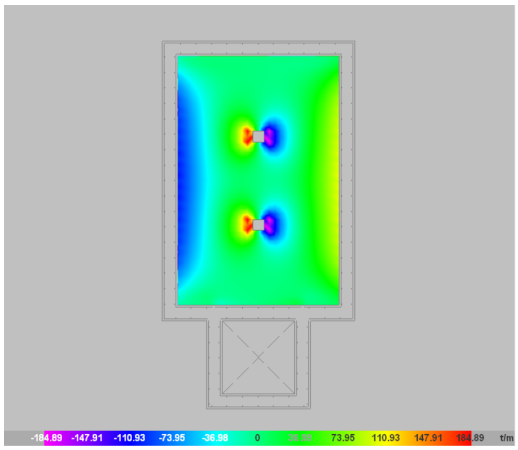

(b) Shear stress, x-direction (t/m)

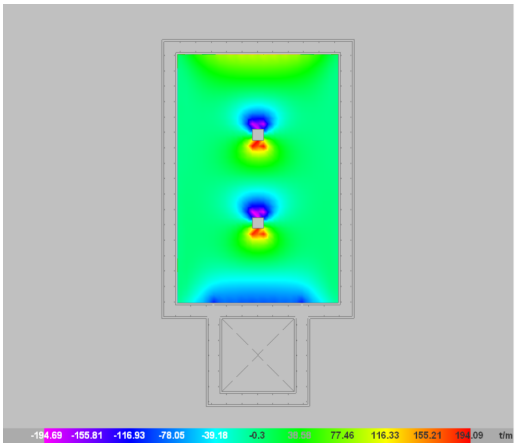

(c) Shear stress, y-direction (t/m)

Figure 34: Total and x,y-direction shear stresses on the upper concrete slab of the Machines Hall.

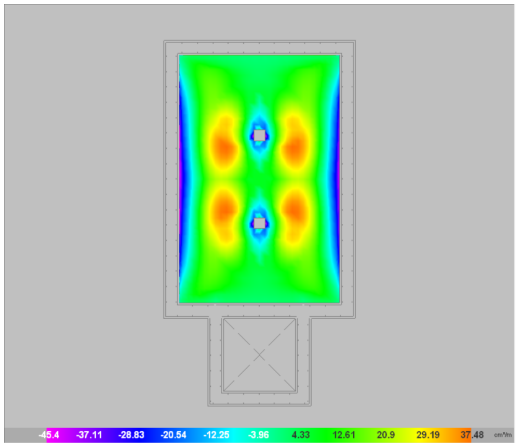

(a) Inferior, x-direction

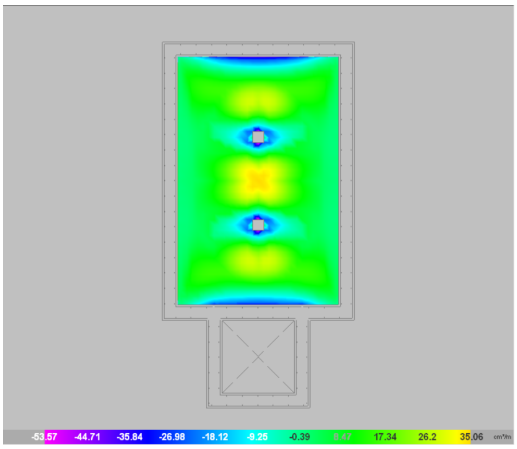

(b) Inferior, y-direction

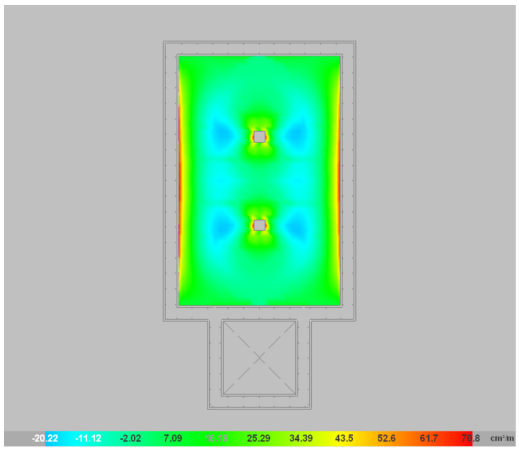

(c) Superior, x-direction

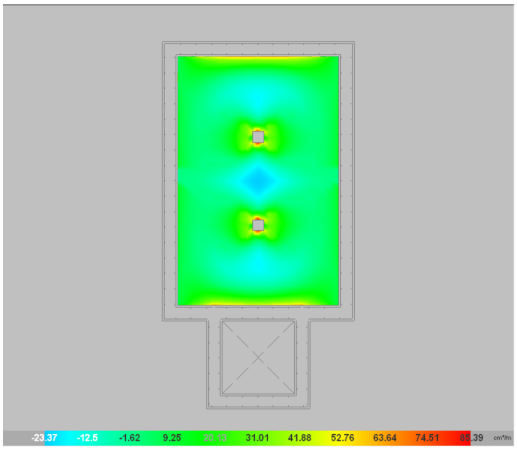

(d) Superior, y-direction

Figure 35: Amount of reinforcement steel required (cm^2/m) for the upper concrete slab of the Machines Hall. Reinforcement considered: superior and inferior reinforcement for both x,y-directions.

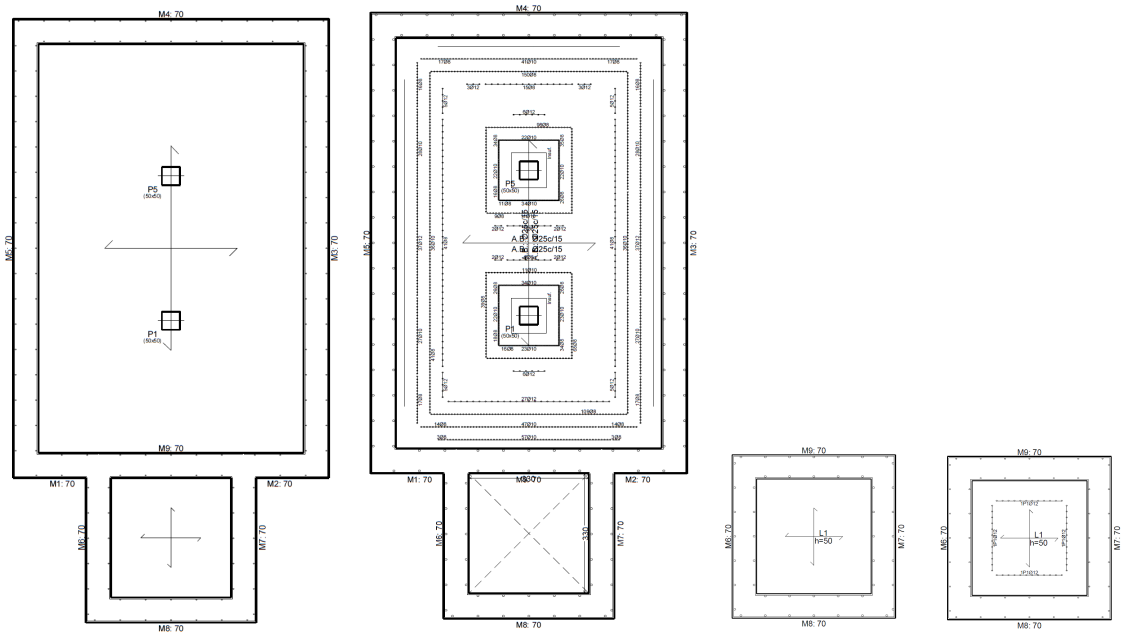

(a) Floor P2 (b) Floor P3 (c) Floor P4 (d) Floor P5

Figure 36: Slab Reinforcement of the project floors P2-P5. Floor P1 is not added because it represents the foundations, it does not contain an horizontal slab.

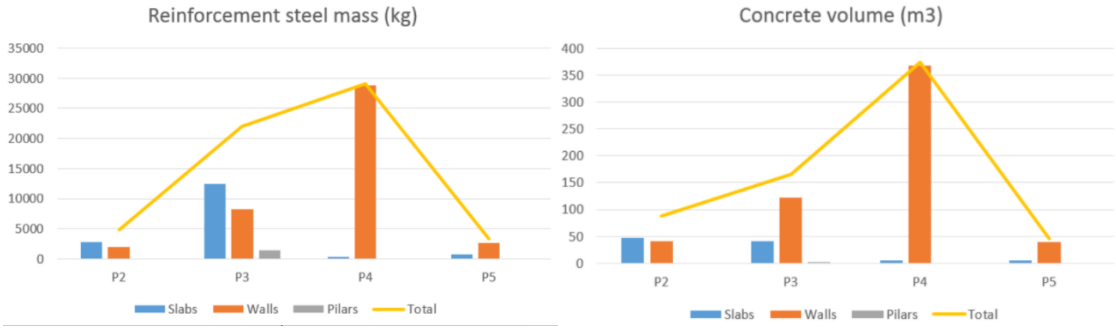

(a) (b)

Figure 37: Decomposition of the steel mass (a) and the concrete volume (b) used in each floor and for each structural component.

12 Discussion

Section 7 presents a detailed methodology for designing some of the components of the Engine Reservoir: the reversible pump/turbine main characteristics, the penstock diameter, the reservoirs capacity and the pump flow rate. It has been observed the relation with the component design variable with the turbine design head, which stresses the relevance of a good design of the turbine design head. Nevertheless, the hydro-power and electrical components characterisation is not complete due to difficulties in finding detailed datasheets of the components.

Once the main components have been characterised, the designs are developed in Section 8. Design I was made before the completion of the hydro-power components characterisation, therefore it does not present a clear distribution or design of the components inside the Machine Hall. Nevertheless, it presents the advantages of more light simulations (highly symmetric) and greater resistance against hydrostatic pressures and lateral earth pressures. As a contrast, Design II presents a detailed design of the Machine Hall for the elements that could be characterised.

Section 6.0.1 describes in detail the main interactions to be modelled and tested in a ordered way. Both the stability conditions, and the seabed and fluid interactions are clearly presented and ready to be implemented in the models. On the other side, the interactions with the Rigid and Flexible Reservoirs are treated in less detailed, and its effects quickly neglected. Although the approximated calculations show they do not cause any significant load that could make the Engine Reservoir loose its stability, there could be significant concentrated loads and momentum on certain regions of the structure, specially on the flow connections with the reservoirs. It could be argued that a depth study on Engine Reservoir connections would be necessary before neglecting the interactions.

Regarding the interactions and structure modelling, Model I provides a clear insight on structure stability on a porous seabed, and provides a useful design criteria (safety factors satisfaction) and design requirement (specified safety factor) to be taken into account in next steps of the design project or in other design projects. Model II and IV verify the expressions from Section 39 regarding the pore pressure, effective vertical pressure and lateral earth stress. Additionally, Model II provides results for soil compression, although it is of few interest for the current design. Model III proves the currents can be discarded at the range of seabed depth of the current design, where hydrostatic pressure is orders of magnitude bigger than the viscous forces caused by the currents. Nevertheless, the data and fitting procedures from Appendix A,B,C might be used for other project that contain solid domains near or partially above the fluid surface.

Model V was a very promising idea, as it took advantage of the COMSOL's ability to combine Physics to unify all the previous models. A mistake on the governing equations or boundary conditions must have been made. As for Model VI, it satisfactorily models the environment interactions with the Design II structure. It is observed a accumulation of error on the ceiling of the Machines Hall and a small tilt along the structure shaft. It is concluded that steel reinforcement is necessary for reducing the bending displacement of the concrete material. On the other side, additional optimisations could be made on the structure geometry at this stages, so that the concrete receives compressing stresses. Design I geometry could be recovered at this point, or a dome-based shape of the Machines Hall geometry might have a better performance.

Finally, Model VII provides detailed results on the structure components and building drawings. Small moments are observed, and the shaft suffers a significantly lower displacement than in the case of no reinforcement. Moreover, the slabs and walls displacements when compared to the no-reinforced model have also decreased. Nevertheless, the resulting design needs too many, it is not economically feasible. It is expected that the geometry optimisation mentioned in the previous paragraph will greatly reduce the high reinforcement requirement of the design.

13 Conclusion

Several goals were defined for the design project. Its evaluation will determine the success of the design project.

The first goal was to identify the Engine Reservoir design requirement. They have been clearly identified in Table 1 and also related to design criteria. Therefore, the first goal has been achieved.

The next goal was to make a preliminary design of the hydropower components. Following the argumentation in the Discussion section, it is though that the goal has been half achieved. On the one side, some components have been described in detail, such as the reversible pump-turbine and the penstock. On the contrary, other components such as the motor and the generator have been characterised using a lot of approximations due to the lack of available data on the flied. Others, such as the transformers, have not been treated. Conclusively, this goal is half achieved.

The third and forth goal were to identify the main interactions between the Engine Reservoir and the fluid, the seabed and the Rigid and Flexible Reservoirs, and to develop a method for the interactions quantification. According to what has been said in Discussion section, the interactions between the Engine Reservoir and the environment are identified and described in detail, and the main governing equations of the interactions are also provided. Additionally, multiple models have been developed that study and simulate the interactions individually, so that the effect of design variables such as the embedded depth on the studied interaction are more easily detected and understood. Nevertheless, the interaction between Engine Reservoir and Flexible and Rigid Reservoir should be treated in more detailed. Specifically for the connection component between the two structures, it should be analysed and tested individually. As a result, the goal is considered achieved for the most part.

Finally, the fifth goal was to elaborate a first design for the Engine Reservoir and to analyse its mechanical performance. Design II has been developed taking into account all the requirements from Tab. 1 and from the hydro-power machines characterisation. Not only the external geometry has been defined, but also the general distribution of the components within the Machine Hall (Fig. 10) and the main structural components (Fig. 17). Additionally, an extensive mechanical analysis has been performed with results regarding the structure displacement, momentum, stress distribution, reinforcement ratio requirement an others (Sec. 11.6). Finally, it is also provided a project summary regarding the materials in total and decomposed in floors and structural components. It has been concluded that the model was not economically feasible due to the large amount of steel used, but the model is very flexible for changes on the structure geometry or material. Then, it is concluded that the fifth goal is reached satisfactorily.

14 Recommendations and Limitations

Along the project, several limitations of the models and the design has been detected. Some of them are caused by lack of information (such as seabed characteristics or machines characteristics) and some of them for the sake of simplifications in the models (one-way interactions). All of them will be explained below, and some recommendations will be made regarding model and design further modifications.

The lack of knowledge on the seabed characteristic is a big limitation of the design. Along the project and specially on the models results, it has been observed a big dependency of the soil type for the uplift stability factor, the lateral earth pressure calculation and the filling soil weight. These parameters have a high effect on the structure design, as for example large lateral earth pressures will require a more robust structure. Therefore, the more information of the soil is provided, the more can the design be optimised.

Also in the field of seabed characterisation, no different soil layers have been treated during the project. One consequence of considering multiple soil layers (of different density and earth pressure coefficient value) would be a change on the earth pressures on the structure boundaries. Another even more drastic change on the model would be the consideration of impermeable layers, which would cause the water pore pressure to suddenly drop, and therefore the earth pressures on the structure surfaces would change drastically. Additionally, all models assume completely saturated soil at all soil depth, although partially saturated soils can also be found.

As for the hydro-power machines characterisation, there is a lot of work left on characterising the parameters. Moreover, the design choice of 4 turbines of 500kW each should be reviewed by taking into account the turbine efficiency with respect to the head, the head variation, the designed head an other turbine parameters that have to be specified in detail to offer the maximum efficiency. The same recommendation applies for the pump and other relevant components of the Engine Reservoir.

A big limitation of the project design is that is has not taken into account the installation and construction processes for the structure design. Literature research should be done on the embedding procedure procedures of large structures. Alternatively, the design in parts of the Engine Reservoir could be considered. Also the transportation process from the shore to offshore and to the bottom of the lake is to be investigated. In conclusion, construction, transportation and installation procedures should be detailed, and the design of the Engine Reservoir might change to adequate to the procedures requirements.

Finally, an economic study should be made for the design of the structure. Specifically, the embedded depth plays an important on machinery characterisation, power production and storage capacity, minimum strength of the structure and so on. The materials summary on Tab. 12 is the first approach to include economical considerations into the design.

References

[1] *Recommended Practice for Planning, Designing and Constructing Fixed Offshore Platforms—Working Stress Design.* American Petroleum Institute.

[2] MMT Group AB. Gephysical Survey. Ten Noorden van de Waddeneilanden Wind Farm Zone. Technical report, Rijksdienst voor Ondernemend Nederland, June 2020.

[3] Anonymous. Epdm rubber. `https://en.wikipedia.org/wiki/EPDM_rubber`. [Accessed in 2-12-2020].

[4] Anonymous. Some useful numbers on the engineering properties of materials (geologic and otherwise). `https://www.jsg.utexas.edu/tyzhu/files/Some-Useful-Numbers.pdf`. [Accessed in 15-10-2020].

[5] DHI A/S. Metocean desk study and database for Dutch Wind Farm Zones. Feasibility level study for IJmuiden-Ver, Ten Noorden van de Waddeneilanden & Hollandse Kust (west). Technical report, Rijksdienst voor Ondernemend Nederland, March 2019.

[6] Prof.Dr. Atil Bulu. *Hydroelectric Power Plants.* Istanbul Technical University.

[7] Ocean Grazer BV. Ocean energy for a sustainable future. `https://oceangrazer.com`. [Accessed in 9-10-2020].

[8] Linyi Solpac Co. Water storage tank flexi bladder food grade drinking water tank. `https://solpac.en.made-in-china.com/product/TNHQeiFdfXhE/China-Water-Storage-Tank-Flexi-Bladder-Food-Grade-Drinking-Water-Tank.html`. [Accessed in 2-12-2020].

[9] D. Coduto. *Foundation design: principles and practices.* Prentice Hall, 2 ed., Upper Saddle River, New Jersey, USA, 2001.

[10] Comsol. Introduction to the porous media flow module. `https://doc.comsol.com/5.5/doc/com.comsol.help.porous/IntroductionToPorousMediaFlowModule.pdf`. [Accessed in 29-10-2020].

[11] Emiliano Cora. Hydropower Technologies: the state-of-the-art. Technical report, Hydropower Europe, August 2019.

[12] CYPE. Cypecad. reliable structures, very precise drawings. `http://cypecad.en.cype.com/`. [Accessed in 1-11-2020].

[13] B. Das. *Principles of Foundation Engineering.* Thomson, 5 ed., Toronto, Ontario, Canada, 2007.

[14] Braja M. Das. *Principles of Geotechnical Engineer, 7th Edition.* Cengage Learning, Stamford, USA, 2010.

[15] Demetri Bouris Efstathios Konstantinidis, Alexis Dedes. Drag and intertia coefficients for a circular cylinder in a steady plu low amplitude oscillatory flow. *10th International Conference on Flow-Induced Vibration (& Flow-Induced Noise)*, pages 473–480, 2012.

[16] R.Ebara K.Yanase F.Kawamura, M.Miura. Material strength of long-term used penstock of a hydroelectric power plant. *Case Studies in Structural Engineering*, 6:103–114, 2016.

[17] Ying Yang Heng Lin, Yiqiang Xiang. Coupled vibration analysis of cfrp cable-tube system under parametric excitation in submerged floating tunnel. *Procedia Engineering*, 166:45–52, 2016.

[18] L.Y. Hut. Investigating the structural behavious of the ocean battery. Master's thesis, Rijksuniversiteit Groningen, the Netherlands, 2020.

[19] American Iron and Steel Institute. *Buried Steel Penstocks*. Steel Plate Fabricators Association, INC, 1998.

[20] Chen Chen Jikai Zhou, Chenghuan Lin and Xiyao Zhao. Reduction of groundwater buoyancy on the basement in weak-permeable/impervious foundations. *Advances in Civil Engineering*, 2019, 2019.

[21] Adityo Kuncorojati. Flod structure detection analysis during inflation and deflation process on bladder reservoir of ocean grazer using 3d finit element method. Master's thesis, Rijksuniversiteit Groningen, the Netherlands, 2020.

[22] K.Webb. ESE 471 – Energy Storage Systems. Section 3: Pumped-hydro energy storage. Technical report, 2016.

[23] S. Bhattacharya Laszlo Arany. Design of monopiles for offshore wind turbines in 10 steps. *Soil Dynamics and Earthquake Engineering*, 2016.

[24] Norconsult. Wind power based pumped storage Pre-Feasibility Study. Technical report, Nordic Council of Ministers, July 2013.

[25] United States Department of the Interior Bureau of Reclamation. Estimating Reversible Pump-Turbine Characteristics. Technical report, December 1977.

[26] Ronald L. Panton. *Incompressible Flow*. John Wiley & Sons, Inc., Hoboken, New Jersey, 2013.

[27] Kenneth Gavin Paul Doherty. The shaft capacity of displacement piles in clay: A state of the art review. *Geotechnical and Geological Engineering*, 29:389–410, 2011.

[28] Ruwan Rajapakse. *Geotechnical Engineering Calculations and Rules of Thumb, Second Edition*. Butterworth-Heinemann, 2016.

[29] E. I. Udechukwu-Ukohah S. C. Ugochukwu, E. A. Nwobu. Regression models for predicting quantities and estimates of steel reinforcements in concrete beams of frame buildings. *Journal of Scientific Research & Reports*, 26:60–74, 2020.

[30] Ethan Shepherd. Chapter 3: Hydraulic turbine classification and selection. Technical report, January 2017.

[31] Wind Energy Solutions. Wes250. `https://windenergysolutions.nl/turbines/windturbine-wes-250/#toggle-id-6`. [Accessed in 28-10-2020].

[32] Anson Steel. Jis g3101 ss400 structural carbon steel plate specification. `http://www.steels-supplier.com/steel-standard/jis-g3101-ss400-structural-carbon-steel-plate-specification.html`. [Accessed in 12-11-2020].

[33] Sulzer. Pumped hydro storage power. `https://www.sulzer.com/-/media/files/applications/power-generation/brochures/pumped_hydro_sstorage_power_e10125.ashx?la=en`. [Accessed in 15-10-2020].

[34] Bogumil Wrana. Pile load capacity - calculation methods. *Studia Geotechnica et Mechanica*, 37(4), 2015.

A Metocean Data

Metocean data refers to data related with meteorology and (physical) oceanography. The meteocean conditions of the design project are the combination of wind, current and wave conditions of the chosen location. The data is categorised as normal sea-state conditions (Tab. 13 and 14) and extreme sea-state conditions (Tab. 15). More thorough and detailed meteocean studies will be required in further phases of the design (out of scope).

Metocean data is extracted from the database generated by Rijksdienst voor Ondernemend Nederland (RVO.nl). The report produced in 2019 called 'Metocean desk study and database for Dutch Wind Farm Zones' gathers metocean data from 15/1/1979 to 1/10/2018 and its pre-processed analysis [5]. The dataset has been published by DHI as 'MIKE 21 Hydrodynamic Model (HD)', and it covers the Dutch Offshore Wind Farms area delimited in Fig. 38. In particular, the tables presented bellow contain the data from the area of Ten Noorden van de Waddeneilanden (TNW) offshore wind farm (associated with number 5 in the figure).

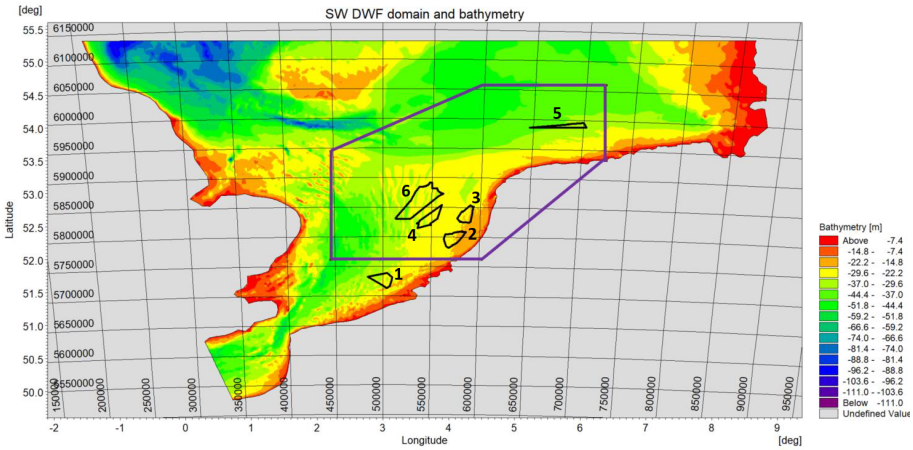

Figure 38: Dataset covered area (delimited with a purple line) and colour-map of the mean water depth (land areas in grey). Included Dutch offshore wind farms (delimited by a black line): Borssele (1), Hollandse Kust zuid (2), Hollandse Kust noord (3), Hollandse Kust west (4), Ten Noorden van de Waddeneilanden (5) and IJmuiden Ver (6) [5].

Depth	Parameter	Mean [m/s]	Min [m/s]	Max [m/s]
Depth-integrated	$u_{tot,depth-int}$	0.3	0.0	1.0
	$u_{tid,depth-int}$	0.3	0.0	0.6
	$u_{res,depth-int}$	0.1	0.0	1.0
Near-surface	$u_{tot,surf}$	0.4	0.0	1.3
	$u_{tid,surf}$	0.3	0.0	0.8
	$u_{res,surf}$	0.1	0.0	1.4
75% of water column	$u_{tot,75\%}$	0.3	0.0	1.1
	$u_{tid,75\%}$	0.3	0.0	0.7
	$u_{res,75\%}$	0.1	0.0	1.2
50% of water column	$u_{tot,50\%}$	0.3	0.0	1.1
	$u_{tid,50\%}$	0.3	0.0	0.6
	$u_{res,50\%}$	0.1	0.0	1.0
25% of water column	$u_{tot,25\%}$	0.3	0.0	0.9
	$u_{tid,25\%}$	0.2	0.0	0.5
	$u_{res,25\%}$	0.1	0.0	0.8
5% of water column	$u_{tot,5\%}$	0.1	0.0	0.5
	$u_{tid,5\%}$	0.1	0.0	0.3
	$u_{res,5\%}$	0.0	0.0	0.5

Table 13: Current velocity data for TNW normal sea state ('Mean') and extreme sea state ('Max'). Current depth average and current velocity profile data for specific percentages of the water column [5].

$H_{S,NSS}$ [m]	$T_{P,NSS}$ [s]		
	5%	50%	95%
1	3.4	5.4	14.6
1.5	4.4	6.0	12.4
2	5.2	6.5	12.1
2.5	5.9	7.1	11.1
3	6.6	7.7	10.9
3.5	7.3	8.2	10.2
4	7.9	8.6	10.4
4.5	8.4	9.1	11.0
5	8.9	9.6	11.4
5.5	9.3	10.1	12.3
6	9.7	10.5	12.3
6.5	10.2	11.1	13.0
7	10.5	11.6	14.1
7.5	11.0	12.5	14.0
8	11.2	13.0	15.0

Table 14: Significant wave height and associated peak wave period for TNW normal sea state. The significant wave height ($H_{S,NSS}$) is discretised by 0.5m steps, and the range of peak wave period ($T_{P,NSS}$) associated to each wave height is presented by the values of 5%, 50% and 95% of the data [5].

Parameter	Symbol	Value	Unit
Extreme total high water level	HWL_m	3.5	m
Extrem total low water level	LWL_m	-1.0	m
Extreme wind speed (10m from MSL and 10min averaged)	$u_{m,10m,10min}$	34.4	m/s
Significant wave height	H_s	9.1	m/s
Maximum wave height	H_m	17.2	m/s
Mean wave period associated to maximum wave height	T_{H_m}	11.8	s

Table 15: TNW metocean extreme values with a 50-years return period [2].

B Hydrodynamic environmental modelling

The design has to take into consideration the environmental conditions that have a bigger impact on its structural behaviour: the currents and the waves. From measurements or model-generated data, two environmental conditions have to be described:

- Normal environmental conditions: it is expected that the normal environmental conditions occur frequently during the service life of the Engine Reservoir.
- Extreme environmental conditions: it is expected that the extreme environmental conditions occur rarely during the Engine Reservoir service life. They constitute the maximum loading of the Engine Reservoir.

The structure is exposed to the sea state currents and waves. The principles that guide this actions and its interaction with the half-buried structures are presented below and they are based on the work made by Kokkinowrachos on ´Hydrodynamik der Seebauwerke´.

B.0.1 Currents modelling

The currents present on the sea are commonly categorised into tidal currents (associated with astronomical tides), wind-generated currents and, if applicable, wave-induced currents and specially breaking waves.
Depending on the location, other currents may be considered, such as the permanent current current (constant velocity over the depth).

The current velocity vector has a spacial and temporal dependency, it can be generally written as $\mathbf{u}_c = \mathbf{u}_c(x, y, z; t)$. The time-dependency that originates flow fluctuations is caused by turbulence. Nevertheless, for most applications the current can be considered as a steady flow, where the current velocity only depends on the depth ($\mathbf{v}_c = \mathbf{v}_c(z)$).

The total current velocity at a given location (x,y) is the vector sum of the each type of current present, and the total current profile describes its speed and direction as a function of the elevation. It should be described for both normal and extreme environmental conditions.

Tidal current
Tidal currents are associated with astronomical tides, they are caused by the gravitational forces of the moon and the sun. They are generally weak on deep waters past the shelf break, and stronger on broad continental shelves. Its normal current values rarely exceed 0.3 m/s along an open coastline When there are no detailed field measurements, the tidal current velocity $v_{c,tidal}$ may be modelled by the following power law equation assuming unidirectional current:

$$u_{c,tidal}(z) = u_{c,tidal}(0) \cdot \left(\frac{d+z}{d}\right)^{\alpha} \qquad \text{for} \quad z \leq 0 \tag{107}$$

where z is the water level, being $z = 0$ the still water level, $u_{c,tidal}(0)$ the tidal current velocity at still water level, d the seabed depth and the exponent is taken generally as $\alpha = 1/7$.

Wind-generated current
The wind-generated current velocity $v_{c,wind}$ may be modelled as a linear profile from $z = d_0$ to still water level:

$$u_{c,wind}(z) = f(x) = \begin{cases} u_{c,wind}(0) \cdot \frac{d_0+z}{d_0} & \text{for} \quad -d_0 \leq z \leq 0 \\ 0 & \text{for} \quad z < -d_0 \end{cases} \tag{108}$$

where the reference depth is generally chosen as $d_0 = \min(d_{mudline}, 50m)$ and the wind-generated current at still water level is given by $u_{c,wind}(0) = 0.015 \cdot v_{10m,1h}$, with $u_{10m,1h}$ being the average over 1h of the wind speed at 10m height above the still water level. Conversely, the wind-generated current from $z = d_0$ to still water level can be taken as a slab profile:

$$u_{c,wind}(z) = f(x) = \begin{cases} u_{c,wind}(0) & \text{for} \quad -d_0 \leq z \leq 0 \\ 0 & \text{for} \quad z < -d_0 \end{cases} \tag{109}$$

From the two expressions of the wind-generated current profile, it has to be applied the profile that gives the highest loads for the Engine Reservoir design.

Wave-generated current
The wave-generated currents, and in particular the surf-generated currents, are to be considered when breaking waves are present on the water surface. The surf-generated current is estimable through numerical models, such as the Boussinesq model. For coastal currents parallel with the line of the coast, the design velocity can be approximated as:

$$u_{c,surf} = 2 \cdot s \cdot \sqrt{g \cdot H_B}, \tag{110}$$

where s is the seabed slope near the shore, and H_B is the height of the breaking wave. The wave-generated current velocities can be determined by the same power law equation as the tidal currents:

$$u_{c,surf}(z) = u_{c,surf}(0) \cdot \left(\frac{d+z}{d}\right)^{1/7} \qquad \text{for} \quad z \leq 0, \tag{111}$$

Superposition of currents
The flow velocity that determines the velocity vertical profile of the sea-water is obtained by the combined action of the previously defined sea currents. For simplicity and safety, the currents are assumed in the same direction, and therefore the total current velocity $u_c(z)$ as a function of the vertical component is obtained by:

$$u_c(z) = U_{c,tidal}(z) + u_{c,wind}(z) + u_{c,surf} \tag{112}$$

B.0.2 Waves modelling

For the wave model, different models should be applied depending on the mean water depth, the wave height and the wave period. The regions of applicability of the main wave theories are shown in Fig. 39. The figure shows their dependency with two dimensionless wave properties: the dimensionless wave steepness $\tilde{H}$ and the dimensionless relative depth $\tilde{d}$:

$$\tilde{H} = \frac{H}{gT^2}, \qquad \tilde{d} = \frac{d}{gT^2} \tag{113}$$

where H is the wave height (m), T is the wave period (s), g is the gravity acceleration (m/s^2) and d is the mean water depth or MWD (m).

Firstly, the applicable wave theory is evaluated for the normal sea state case. Using Eq. 113 and mean water depth $d = 35m$, the metocean data for normal sea state conditions ($H = H_{S,NSS}$ and $T = T_{P,NSS}$ from Tab. 14) is used to compute$\tilde{H}$ and $\tilde{d}$. They are compared with the regions of applicability of Fig. 39, and it is obtained the applicable wave theory for every condition considered. The results are summarised in Tab. 16, from which it is concluded that he waves of the normal sea state should be modelled using Stokes 5th order or Stream Function.
Secondly, the extreme case is considered. From Tab. 15, the extreme wave parameters are $H = H_m = 17.2m/s$, $T = T_{H_m} = 11.8s$ and $d_{HWL} = d + HWL_m = 38.5m$ and $d_{LWLL} = d + WHL_m = 34m$. Substituting the extrem values in Eq. 113, it is obtained $\tilde{H}_m = 0.0126$ and $\tilde{d}_{m,HWL} = 0.028$ and $\tilde{d}_{m,HWL} = 0.025$ for the case of extreme total high wave level and low wave level respectively. Comparing the results with the regions of applicativity of Fig. 39, it is obtained that the fluid particle motion may be computed using Stokes 5th order and Stream Function 3rd order. are also appropriate for the extreme sea state.
Therefore, the decision on the wave model to use for the design wave loads modelling is dependent on the location and wave data.

H [m]	T [s]	$\tilde{H}$	$\tilde{d}$	Region of applicability
1	3.4	0.0088	0.309	Stokes 5th order / Stream Function 3rd order
1	5.4	0.0035	0.122	Stokes 5th order / Stream Function 3rd order
1	14.6	0.0005	0.017	Stokes 5th order / Stream Function 3rd order
4.5	8.4	0.0065	0.051	Stokes 5th order / Stream Function 3rd order
4.5	9.1	0.0055	0.043	Stokes 5th order / Stream Function 3rd order
4.5	11.0	0.0038	0.029	Stokes 5th order / Stream Function 3rd order (limit)
8	11.2	0.0065	0.028	Stokes 5th order / Stream Function 3rd order
8	13.0	0.0048	0.021	Stokes 5th order / Stream Function 3rd order
8	15.0	0.0036	0.016	Stokes 5th order / Stream Function 3rd order (limit)

Table 16: Computation of dimensionless wave steepness ($\tilde{H}$) and relative depth ($\tilde{d}$) for the case of normal sea states. Results for the lowest, intermediate and largest significant wave height and their associated peak wave periods (Tab. 14).

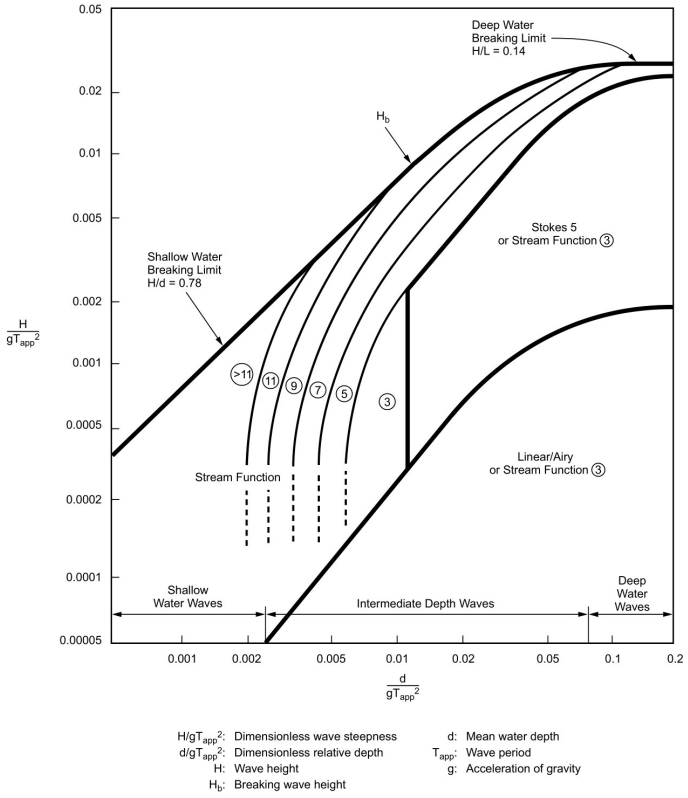

Figure 39: Regions of applicability of different wave theories as a function of the dimensionless wave steepness (H/gT_{app}^2) and the dimensionless relative depth (d/gT^2). The wave theories considered are Stream Function, Stokes V and Linear Wave Theory [1]

C Velocity profile fitting for normal and extreme state conditions

From normal and extreme sea states, current input data (Tab. 13 have been used to fit nonlinear models. It is direct to see from the tables that the current is mainly caused by tidal currents; this observation will influence in the proposed nonlinear models for the current profile. Additionally, it has been imposed null current velocity at mudline depth to satisfy the boundary conditions between fluid and seabed sub-models (referred in the figure as 'mudline condition').

The nonlinear models expressions have been extracted from Section B.0.1. In both cases (normal and extreme sea states), two different procedures are used to fit the data. Nonlinear model #1 is constructed by firstly fitting the tidal current data (u_{tid}) from Tab. 13 to the theoretical tidal current expression (Eq. 114), and secondly using the total current data to fit the total current model (Eq. 115), where c_1, α have been already determined in the first fitting procedure. Then, the model #1 is characterised by coefficients c_1, α and c_2 as:

$$u_{tidal}(z) = c_1\Big(\frac{d+z}{d}\Big)^{\alpha} \tag{114}$$

$$u_{total}(z) = u_{tidal}(z) + c_2\Big(\frac{d+z}{d}\Big) \tag{115}$$

Conversely, the nonlinear model #2 is directly defined as:

$$u_{total}(z) = c_1\Big(\frac{d+z}{d}\Big)^{\alpha}, \tag{116}$$

where coefficients c_1 and α have to be fitted.

The results of the fitting are shown in Fig. 40, and summarised in Tab. 17,18. From the comparison of the Root Mean Square Error and Adjusted R-Squared Error, it has been chosen Model #1 for mean current velocity expression, and Model #2 for the case of maximum current velocity. Then, the velocity profile for normal sea-state is calculated using Eq. 117 ($u_{nss}(z)$), and extreme sea-state is obtained from Eq. 118 ($u_{ess}(z)$):

$$u_{nss}(z) = 0.33\Big(\frac{35+z}{35}\Big)^{0.34} + 0.06\Big(\frac{35+z}{35}\Big) \tag{117}$$

$$u_{ess}(z) = 1.28\Big(\frac{35+z}{35}\Big)^{0.29} \tag{118}$$

$$\tag{119}$$

	Model #1	Model #2
Fitted coefficients	$c_1 = 0.33, \alpha = 0.34, c_2 = 0.06$	$c_1 = 0.38, \alpha = 0.34$
Root Mean Square Error	0.0424	0.0439
Adjusted R-Squared Error	0.921	0.915

Table 17: Fitted coefficients and fitting errors of the nonlinear models regarding the mean current velocity.

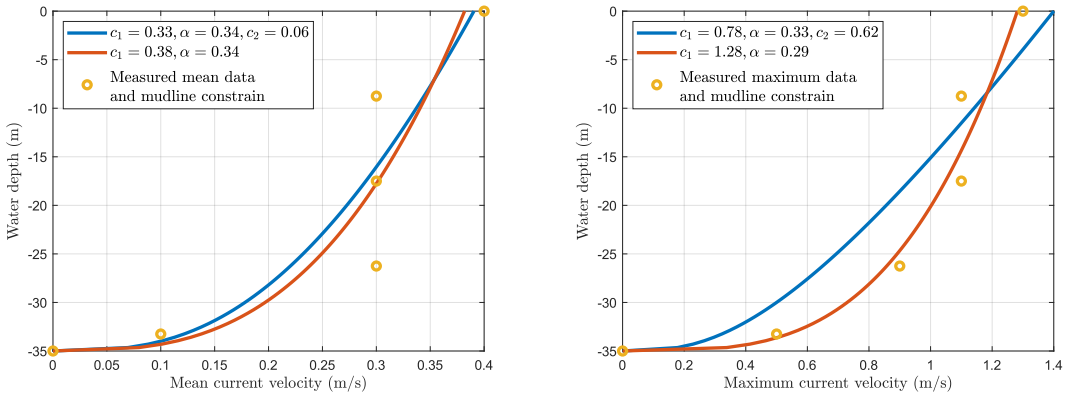

(a) Mean current velocity

(b) Maximum current velocity

Figure 40: Measured current velocity profiles (orange circles, data from Tab. 13) and predicted velocity profiles (continue curves). The velocity profiles have been predicted using the nonlinear model from Eq. 114,115 (blue) and from Eq. 116 (red)

	Model #1	Model #2
Fitted coefficients	$c_1 = 0.78, \alpha = 0.33, c_2 = 0.62$	$c_1 = 1.28, \alpha = 0.29$
Root Mean Square Error	0.166	0.056
Adjusted R-Squared Error	0.882	0.987

Table 18: Fitted coefficients and fitting errors of the nonlinear models regarding the maximum current velocity.